

From Indoor to Open World: Revealing the Spatial Reasoning Gap in MLLMs

Mingrui Wu¹ Zhaozhi Wang¹ Fangjinhua Wang²
 Jiaolong Yang³ Marc Pollefeys² Tong Zhang^{1*}

¹University of Chinese Academy of Sciences ²ETH Zürich ³Microsoft Research Asia

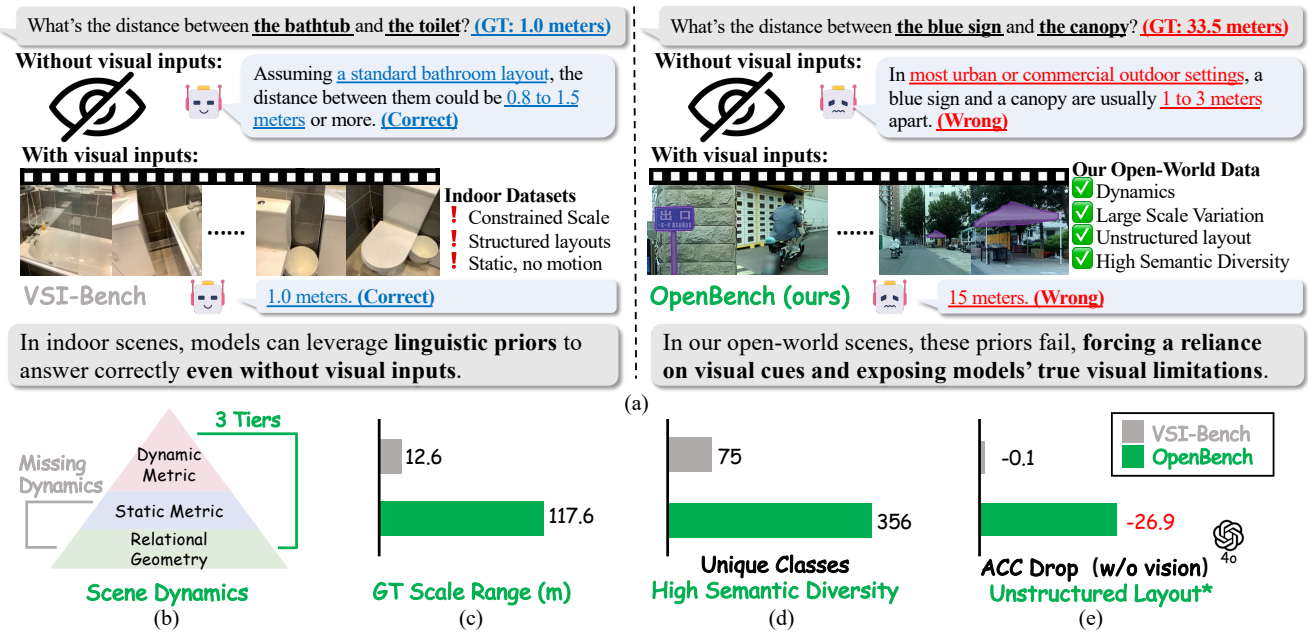


Figure 1. **Comparison between VSI-Bench [65] and OpenBench (ours).** **Top:** Qualitative comparison of Gemini-2.5-Pro’s responses, with and without vision inputs, on VSI-Bench and OpenBench. **Bottom:** Quantitative comparison of two benchmarks in terms of evaluation coverage, scale range, semantic diversity, and accuracy drop without vision inputs. *The mean relative accuracy drop of GPT-4o on absolute distance tasks when vision inputs are disabled. A larger drop proves reliance on vision, not linguistic priors, in the unstructured layouts.

Abstract

While Multimodal Large Language Models (MLLMs) have achieved impressive performance on semantic tasks, their spatial intelligence—crucial for robust and grounded AI systems—remains underdeveloped. Existing benchmarks fall short of diagnosing this limitation: they either focus on overly simplified qualitative reasoning or rely on domain-specific indoor data, constrained by the lack of outdoor datasets with verifiable metric ground truth. To bridge this gap, we introduce a large-scale benchmark built from pedestrian-perspective videos captured with synchronized stereo cameras, LiDAR, and IMU/GPS sensors. This dataset provides metrically precise 3D information, enabling the automatic generation of spatial reasoning

*Corresponding author.

questions that span a hierarchical spectrum—from qualitative relational reasoning to quantitative metric and kinematic understanding. Evaluations reveal that the performance gains observed in structured indoor benchmarks vanish in open-world settings. Further analysis using synthetic abnormal scenes and blinding tests confirms that current MLLMs depend heavily on linguistic priors instead of grounded visual reasoning. Our benchmark thus provides a principled platform for diagnosing these limitations and advancing physically grounded spatial intelligence. Project page: <https://mingrui-wu.github.io/openbench/>

1. Introduction

Multimodal Large Language Models (MLLMs) [2, 3, 6, 14, 26, 28, 33, 42, 44, 57, 58, 60, 76] have emerged as pivotal tools for interpreting and reasoning about the visual world,

Benchmark	Input Modality	Relational	Metric-Static	Metric-Dynamic	Scene	Metric GT Source
OmniSpatial [29]	Single-view	✓	✗	✗	Internet Mixed	N/A
SpatialBench [10]	Single-view	✓	✗	✗	Embodied	MDE [†] , only auxiliary
SparBench [73]	Multi-view	✓	✗	✗	Indoor	N/A
All-Angles-Bench [69]	Multi-view	✓	✗	✗	Indoor	N/A
MMSI-Bench [67]	Multi-view	✓	✗	✗	Internet Mixed	N/A
SpaCE-10 [25]	Video + Pointcloud	✓	✗	✗	Indoor	Off-the-shelf Datasets [7, 17, 70]
SpatialRGPT-Bench [15]	Single-view	✓	✓	✗	Internet	MDE [†]
Open3D-VQA [74]	Single-view	✓	✓	✗	UAV	MDE [†]
CA-VQA [18]	Multi-view	✓	✓	✗	Indoor	Off-the-shelf Datasets [7] + MDE [†]
Ego3D-Bench [24]	Multi-view	✓	✓	✗	Autonomous	Off-the-shelf Datasets [9, 12, 54]
VSI-Bench [65]	Video	✓	✓	✗	Indoor	Off-the-shelf Datasets [7, 17, 70]
STI-Bench [37]	Video	✓	✓	✓	Indoor&Autonomous	Off-the-shelf Datasets [17, 54, 72]
OpenBench (ours)	Video/Stereo Video	✓	✓	✓	Open-World	Metric accurate sensors (Stereo, LiDAR & IMU)

Table 1. **Comparison of benchmarks for spatial intelligence evaluation.** Our benchmark is the first to provide metrically-sound ground truth for all three tiers of spatial intelligence in diverse scenarios. A parallel stereo-input version of the benchmark, featuring the same questions, is also provided to support future research. [†] MDE: Monocular Depth Estimation.

achieving state-of-the-art performance in a wide range of semantic understanding tasks such as visual question answering [1] and image captioning [43]. Building upon this success, recent research has sought to extend these models from semantic to spatial understanding—cultivating spatial intelligence [65], a capability essential for physically grounded AI systems such as autonomous driving [63] and embodied agents [36, 55].

Developing meaningful benchmarks is essential for accurately characterizing the spatial capabilities of MLLMs and guiding future advances. To provide a clear conceptual foundation, we formalize spatial intelligence as a three-level hierarchy of increasing complexity: 1) *Relational Reasoning*, the qualitative understanding of spatial configurations including relative arrangement, orientation, and overall scene structure; 2) *Metric Reasoning*, the quantitative estimation of absolute geometric properties such as distance, depth, and size; 3) *Kinematic Reasoning*, the metric-aware understanding of scene dynamics, encompassing both object motion (e.g., velocity) and the observer’s ego-motion.

This hierarchy helps to contextualize the state of existing evaluations. Nevertheless, most existing benchmarks [29, 69, 73] remain confined to qualitative relational reasoning, without addressing the core challenges of metric and kinematic understanding. Several recent efforts [37, 65] have advanced towards static quantitative evaluation, yet they are restricted to indoor scenes, where 3D meshes [7, 17, 70] provide convenient ground truth. However, such scenes are limited in spatial scale, semantic diversity, and visual variability—rendering the evaluations unrepresentative of real-world conditions. Other attempts [15] have explored outdoor scenarios using monocular images with pseudo-ground-truth depth derived from single-view estimation [66], but these suffer from scale ambiguity [27] and unreliable metric supervision. Compounding these issues, most MLLMs are pretrained on indoor or

web-collected image datasets, raising the critical question: Do current models truly generalize their spatial knowledge to open-world environments?

To address these limitations, we construct a novel open-world benchmark designed to rigorously assess spatial intelligence under real-world conditions. Our dataset comprises high-resolution, pedestrian-perspective videos offering high diversity, covering over 200 distinct outdoor places. To ensure metrically precise supervision, data were collected using a multi-sensor rig combining synchronized *stereo cameras*, *high-precision LiDAR*, and *IMU/GPS sensors*. Building on this, we introduce an automatic pipeline to extract spatio-temporal information and generate comprehensive question–answer evaluations spanning all three tiers of the spatial hierarchy: relational reasoning, metric reasoning, and crucially, kinematic reasoning.

Extensive evaluations of leading open- and closed-source MLLMs on OpenBench yield conclusions that there are no evident improvement of spatial intelligence in open-world settings. First, the metric reasoning ability of current MLLMs is largely superficial—driven by linguistic priors rather than genuine visual perception. As shown qualitatively in Fig. 1 (a) and quantitatively in Fig. 1 (e), our blinding test shows that the accuracy barely drops in the indoor VSI-Bench [65], indicating limited usage of visual cues. Second, MLLMs fail to generalize the spatial knowledge acquired in constrained indoor environments to the complexities of the open world. Models that achieve large gains on indoor spatial benchmarks [65] show negligible improvement on OpenBench, suggesting overfitting to indoor regularities rather than true spatial intelligence. Third, even the strongest models that approach human-level performance on static metric tasks collapse entirely on dynamic reasoning, revealing a fundamental deficiency in quantitative motion understanding.

In a nutshell, our key contributions are summarized as:

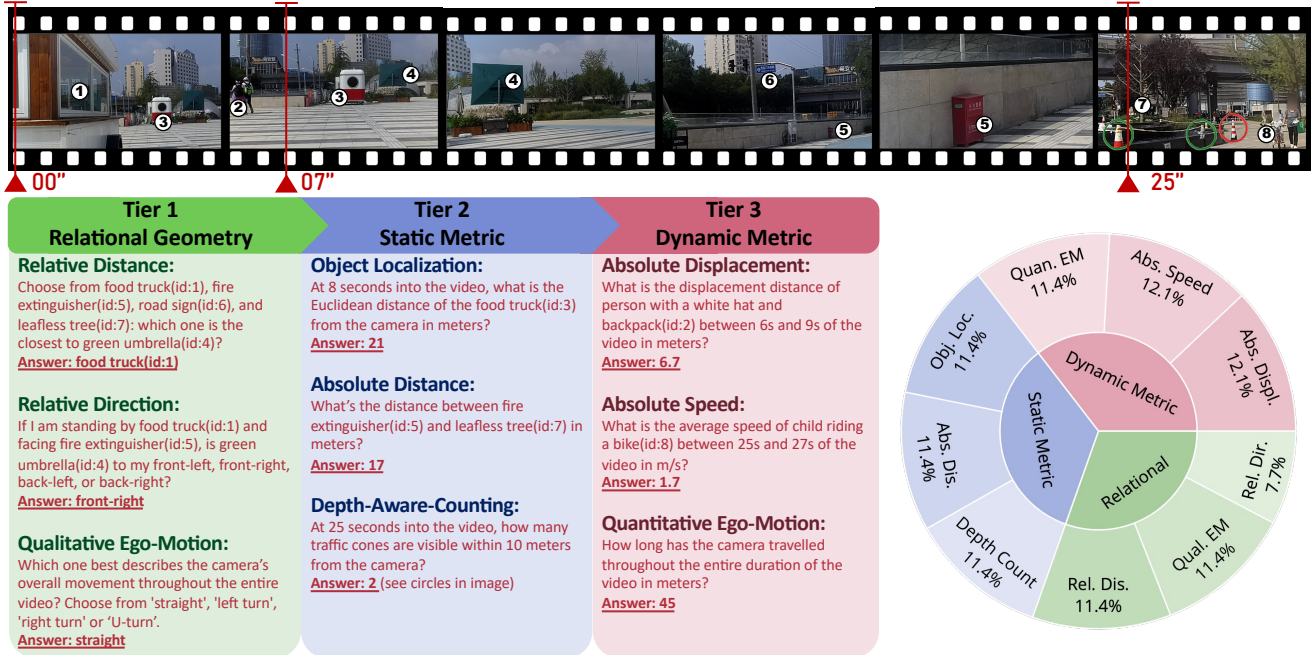


Figure 2. **Tasks and composition of our OpenBench.** (Left) Representative question-answer examples for our three tiers. (Right) Illustration of the final task distribution, which is balanced across both tiers and tasks.

- **A benchmark and dataset for spatial intelligence.** We introduce OpenBench, a metrically precise outdoor benchmark built from multi-sensor pedestrian-view data, with 8,736 question-answer pairs. We will also release additional raw multimodal videos.
- **Comprehensive evaluation of state-of-the-art (SoTA) MLLMs.** We conduct an extensive analysis of leading open- and closed-source models, offering the first unified assessment of spatial reasoning across static, relational, and dynamic tasks under real-world conditions.
- **Current spatial intelligence is fragile.** Our findings reveal that existing MLLMs lack generalizable spatial intelligence—their gains on indoor benchmarks do not transfer to open-world settings.

2. Benchmark

2.1. Overview

Unlike previous works [37, 65] that primarily repurpose off-the-shelf datasets, OpenBench first establishes a purpose-built data foundation through a customized multi-sensor data collection effort that provides metrically-sound ground truth. Second, we designed a pipeline that extracts spatial information and generates question-answer pairs covering the full spectrum of spatial intelligence, finalized by a careful human curation phase to ensure benchmark quality.

The tasks in OpenBench are structured as a hierarchy of three tiers, representing a progression of spatial reasoning capabilities. Fig. 2 provides a detailed breakdown

of the task hierarchy and representative examples at each level. The hierarchy begins with **Relational Reasoning** (relative distance, relative direction, and qualitative ego-motion), which assesses a model's foundational ability to form a qualitative, non-metric spatial representation of the scene. The second tier, **Metric Reasoning**, comprising object localization, absolute distance, and depth-aware counting, introduces a more demanding challenge: grounding visual perception in an absolute metric scale to enable precise, quantitative estimation of static properties like distance. Finally, **Kinematic Reasoning** includes tasks such as absolute displacement and speed estimation. These require maintaining spatio-temporal consistency by tracking entities over time and understanding metric measurements and temporal intervals to compute dynamic quantities.

2.2. Data collection

Platform. Our customized data collection platform, shown in the upper left of Fig. 3, is equipped with a stereo RGB camera system, a 32-beam LiDAR, and an IMU/GPS unit, all of which provide timestamp-synchronized data streams. To ensure smooth motion, the platform is mounted on a manual cart navigated by walking operators.

Data Processing and Curation. Our collection resulted in terabytes of raw data, which were then processed to generate a multimodal dataset. First, stereo images, point clouds, and IMU/GPS data were extracted with timestamps and carefully calibrated. Then LiDAR points were projected to generate sparse depth maps. At last, all sequences were

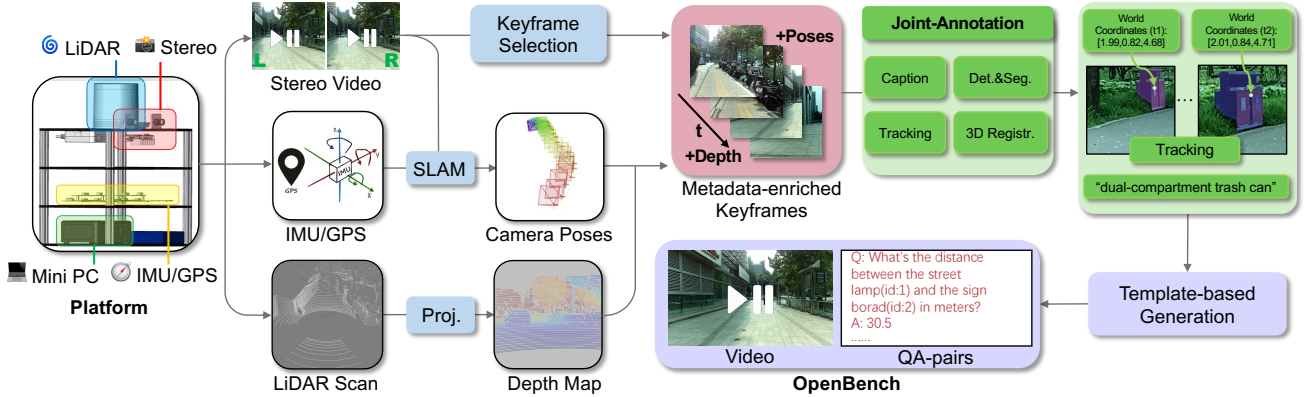


Figure 3. Overview of our benchmark construction pipeline.

manually reviewed for quality, yielding approximately 20 hours of curated high-quality data.

Scene Selection. Our scene selection strategy is designed to ensure environmental diversity while maintaining a strictly pedestrian-centric perspective, not road-centric. To this end, our data collection spans a wide range of sites, including university campuses, public parks, open plazas, and historical sites. This pedestrian-centric perspective of open-world scenes, rarely represented in current MLLM evaluations, not only provides a critical complement to the field but also fulfills our objective of challenging linguistic priors in such unstructured environments. Please refer to Sec. B in the supplementary material for details of data collection.

2.3. Benchmark Construction

We design a three-stage pipeline that transforms raw multimodal data into question–answer pairs. The stages include: (1) Data Preprocessing, (2) Spatial Information Extraction, and (3) QA Generation and Curation. An overview of the entire pipeline is illustrated in Fig. 3. Please refer to Sec. C in the supplementary material for more details and Sec. D for an error analysis of this pipeline.

Stage 1: Data Preprocessing

This initial stage transforms the raw multimodal recordings into a structured format for analysis. First, the data is segmented into shorter video clips, with all streams aligned by their timestamps. From this synchronized data, we generate two streams of geometric metadata: 1) a metric-scale camera pose for each frame is estimated using ORB-SLAM3 [11] from stereo images and IMU data, and 2) a sparse depth map is created by projecting the calibrated LiDAR point clouds onto the image plane. At last, we sample keyframes at a fixed interval from each clip and bundle them with their corresponding camera poses and depth maps. This process yields the **metadata-enriched keyframes** that serve as the primary input for the subsequent stage.

Stage 2: Spatial Information Extraction

We then employ a **Joint-Annotation Module** that inte-

grates multiple expert models to extract semantic and 3D spatial information from the keyframes. A locally-run MLLM first identifies objects and generates textual descriptions, which guide detection and segmentation models to produce pixel-level masks. These masks are temporally tracked using a point-tracking model (e.g., CoTracker [31]) for motion consistency. Each object’s 3D point cloud is subsequently reconstructed from depth maps and registered in the world coordinate system using the estimated camera pose. Consequently, every object is represented by a structured spatio-temporal profile that combines a detailed caption with a continuous 3D trajectory.

Stage 3: QA Generation and Curation

Finally, we convert the extracted structured spatio-temporal information into the final, high-quality video-QA benchmark. Specifically, we first resolve object ambiguity in open-world scenes (e.g., multiple identical street lamps) by assigning each queried object a unique numerical ID, which is overlaid as a visual tag that consistently tracks the object throughout the video. All metric quantities (e.g., distance, speed) are then computed directly from the objects’ spatio-temporal coordinates. Using these annotations, we generate QA pairs through a template-based approach. The automatically generated QA pairs are subsequently refined via an MLLM-assisted, human-in-the-loop curation process. From this curated pool, we sample 1,000 video clips and nearly 1,000 verified QA pairs for each of the nine tasks, ensuring balanced coverage across the three reasoning tiers. The resulting benchmark, OpenBench, comprises 8,736 high-quality QA pairs in total.

3. Evaluation

3.1. Evaluation Setup

Benchmark Models. We evaluate a broad spectrum of MLLMs across various architectures and scales, covering both leading proprietary and publicly available models. All experiments are conducted using the VLMEvalKit [21] to ensure a standardized evaluation protocol. Human per-

Methods	Rank	Avg.	Relational (\mathcal{MCA})		Static Metric (\mathcal{NA})			Dynamic Metric (\mathcal{NA})			
			Rel. Dis.	Rel. Dif.	Qual. EM	Obj. Loc.	Abs. Dis.	Depth Count	Abs. DispL.	Abs. Speed	Quan. EM
<i>Against Human on tiny</i>											
Human-level	1	60.3	85.7	83.3	73.7	43.9	39.2	67.5	42.9	65.8	66.8
Gemini-2.5-Pro	2	36.8	53.1	23.1	46.7	39.7	33.8	40.3	22.2	27.8	40.0
GPT-5	4	27.9	37.5	30.8	40.0	35.3	25.3	12.8	9.2	31.4	33.0
Qwen3VL-32B-Instruct	3	31.9	56.3	23.1	33.3	26.2	10.9	32.8	14.4	37.2	52.3
<i>Closed-source Models</i>											
Gemini-2.5-Pro	1	37.2	50.0	28.1	52.5	37.4	28.1	37.9	26.8	31.1	40.8
Gemini-2.5-Flash	6	19.5	17.9	2.8	50.6	22.7	16.1	26.8	8.1	6.8	20.0
GPT-5	2	29.7	34.4	33.1	49.5	32.5	23.7	20.9	10.5	33.8	30.6
GPT-4o	5	25.9	30.8	29.1	42.2	22.9	27.0	21.6	17.5	15.5	28.8
Claude-3.7-Sonnet	4	26.5	38.9	32.8	47.6	31.3	22.4	31.5	5.2	30.1	5.0
Doubaob-Seed-1.6V	3	27.3	35.9	24.1	44.0	16.6	18.9	38.7	25.7	31.8	9.2
<i>Open-source Models</i>											
InternVL2-8B	14	24.5	35.1	31.7	40.8	21.8	17.8	39.7	15.0	17.8	3.8
InternVL2-40B	16	22.9	36.7	21.0	41.9	21.1	19.2	33.0	10.0	22.0	1.7
InternVL3.5-2B	18	21.7	34.8	32.1	40.1	3.8	2.7	40.8	11.5	16.6	17.0
InternVL3.5-4B	15	23.7	37.6	32.8	44.8	4.6	6.7	40.7	15.6	23.4	10.7
InternVL3.5-8B	4	28.5	37.6	33.6	47.3	12.2	13.2	42.3	20.3	30.2	21.5
InternVL3.5-14B	4	28.5	40.3	33.9	47.1	15.5	15.6	42.8	21.8	32.1	9.0
InternVL3.5-38B	8	26.9	40.2	34.0	45.3	11.6	7.7	42.7	20.3	31.4	11.1
Qwen2.5VL-32B-Instruct	3	30.0	41.7	32.7	44.4	23.9	24.0	27.7	16.7	32.8	27.3
Qwen2.5VL-72B-Instruct	11	26.5	38.5	20.1	46.5	27.7	26.0	29.4	9.4	29.7	9.8
Qwen3VL-2B-Instruct	21	18.4	33.7	32.4	37.5	2.2	4.2	22.4	6.6	19.0	12.5
Qwen3VL-4B-Instruct	19	21.1	34.8	23.7	46.4	3.9	6.9	24.1	13.6	20.4	17.5
Qwen3VL-8B-Instruct	2	31.2	38.3	31.2	49.3	21.0	15.1	33.3	21.3	34.3	37.8
Qwen3VL-32B-Instruct	1	32.2	41.9	28.8	47.1	25.3	11.5	30.2	18.6	36.8	49.2
LLaVA-OneVision-0.5B	20	19.6	27.9	23.8	40.8	13.5	13.1	19.9	10.3	13.6	15.7
LLaVA-OneVision-7B	13	25.7	35.1	32.7	40.8	16.1	25.5	25.6	16.8	28.3	13.4
LLaVA-OneVision-72B	8	26.9	38.6	32.2	41.7	19.6	18.3	35.3	19.2	23.0	16.6
LLaVA-Video-Qwen2-7B	16	22.9	37.1	31.2	40.9	17.6	22.1	18.2	17.5	19.0	5.7
LLaVA-Video-Qwen2-72B	6	28.3	39.8	31.1	42.2	23.5	18.0	34.2	20.7	29.9	17.0
Ovis2-4B	12	25.9	34.6	30.3	40.1	16.1	18.6	36.8	17.7	22.6	18.7
Ovis2-16B	7	28.1	37.0	35.8	42.0	20.0	6.2	41.7	21.7	23.3	28.2
Ovis2-34B	10	26.8	37.3	35.5	40.8	19.1	13.1	37.5	18.7	27.4	15.5

Table 2. **Evaluation results for MLLMs.** We highlight the best and second-best results for each sub-task in **deeper gray** and **light gray**.

formance is evaluated on a 270-question subset. For a fair comparison, we also report the results of several top-performing models on this same subset.

Evaluation Metrics. The tasks in OpenBench are divided into two formats based on their expected answers: Multiple-Choice Answer (\mathcal{MCA}) and Numerical Answer (\mathcal{NA}). For \mathcal{MCA} tasks, we report standard *Accuracy*, and the random baseline is 25.0. For \mathcal{NA} tasks, we primarily follow previous works [22, 65] and employ *Mean Relative Accuracy* (\mathcal{MRA}). Please refer to Sec. E.1 and E.2 in the supplementary material for detailed models and metrics, and E.3 for human evaluation setup.

3.2. Main Results

The main results of our evaluation are summarized in Tab. 2. All models perform far below human-level accuracy, highlighting a pervasive difficulty in reasoning about spatial relations and perceiving the world in a metrically grounded manner. Among all evaluated systems, the closed-source Gemini-2.5-Pro demonstrates a clear performance advantage, achieving the highest scores across five of the nine tasks. Within the open-source category, Qwen3-VL-32B stands out as the strongest model, achieving the best overall

performance within this category.

Unlike prior indoor spatial benchmarks—such as All-Angles-Bench [69] and VSI-Bench [65]—which largely focus on recognition and linguistic reasoning, OpenBench emphasizes the metric perception and reasoning by clearly dividing the overall tasks into 3 tiers. The following findings highlight key behaviors of current MLLMs under this setting, revealing their significant weaknesses in fine-grained metric reasoning.

Finding 1: Human-model disparity peaks on spatial relations rather than on metric estimation.

Humans outperform models most dramatically on relational reasoning tasks (*e.g.*, *relative direction*: 83.3 vs. 23–30 for top models), while the performance gap narrows on metric estimation tasks (*e.g.*, *absolute distance*, *depth-aware-counting*). This indicates that what appears “intuitive” for humans—understanding relative spatial layouts—remains highly non-trivial for current MLLMs. Unlike indoor benchmarks, which primarily expose perceptual or recognition deficiencies, OpenBench surfaces a **cognitive gap** in relational reasoning, underscoring its diagnostic

value for assessing true spatial understanding.

Finding 2: Performance on OpenBench is not uniformly consistent; rather, models exhibit distinct performance profiles with clear strengths and weaknesses that are often specific to the model family.

Beyond the top-performing Gemini-2.5-Pro, we find that model performance lacks a clear correlation between overall scores and specific sub-task capabilities. For instance, while Qwen3VL-32B-Instruct is the leading open-source model on average, it performs poorly on specific tasks, ranking 18th out of 20 on *relative direction* and 15th on *absolute distance*. Moreover, we observe strong task specializations that appear to be inherent to model families. For instance, the OVIS family consistently excels at *relative direction*, and the InternVL3.5 family demonstrates a significant and persistent advantage in *depth-aware-counting*, with all its variants scoring above 40 on this task.

Finding 3: MLLMs fail to reason about quantitative spatial dynamics. While performance on static spatial tasks varies across models, Dynamic Metric reasoning remains a universal failure case.

The top tier of spatial understanding involves estimating dynamic motion in the real world—a task requiring both metric precision and temporal consistency. Unlike static metric reasoning, where Gemini-2.5-Pro performs comparably to human annotators, all evaluated models exhibit a severe degradation when estimating motion-related quantities such as displacement or speed. This result reveals that current MLLMs lack a coherent representation of spatio-temporal continuity and struggle to integrate motion cues across frames. Rather than measuring an incremental weakness, this finding exposes a fundamental limitation of current vision-language architectures and highlights dynamic spatial reasoning as a critical next frontier for research.

Finding 4: The spatial intelligence observed on indoor benchmarks is largely a mirage—unable to transfer to open-world settings.

Multiple recent models [58, 60] report dramatic performance gains on indoor spatial benchmarks like VSI-Bench [65] compared to their predecessors in the same model family. As shown in Fig. 4 (a), newer versions consistently outperform older ones by a substantial margin (e.g., +24.1 gain of InternVL3.5-38B to InternVL2-40B). As noted in InternVL3.5’s technical report [60], more spatial QA data similar to the benchmarks are included, which we posit may explain the observed progress. However, this progress fails to transfer to our open-world OpenBench, as shown in Fig. 4 (b); newer model versions show only marginal performance gains over their predecessors. Notably, on the *absolute distance* task, which we adopt be-

cause its question templates are identical to those in VSI-Bench for a fair comparison and because measuring distance is a principled core ability of spatial perception, the newer InternVL3.5 models consistently underperform their InternVL2 predecessors (see Fig. 4 (c)). This provides more direct evidence that these generalist models are not acquiring generalizable spatial intelligence, but are instead overfitting to the statistical patterns of the indoor benchmarks.

4. Linguistic priors or vision evidence?

After obtaining the main results, we perform additional ablation studies to uncover the underlying sources of failure. In this section, we first examine how current MLLMs rely heavily on linguistic priors rather than visual evidence when reasoning about spatial properties. Building on these observations, we then outline potential directions for developing models with more robust and explicit spatial perception.

4.1. Linguistic priors

We posit that current general-purpose MLLMs fundamentally lack **metric spatial perception**. When presented with spatial tasks, they do not estimate geometric quantities—such as depth, distance, or physical size—directly from visual input. Instead, they approximate these values by drawing on linguistic priors and making semantic comparisons to familiar object categories. To validate the above hypothesis, we conduct two ablation studies below.

Blinding Tests. To examine the extent to which models genuinely rely on visual evidence, we evaluate them under a blinding setup where visual inputs are removed while the textual questions remain unchanged. As displayed in Tab. 3, most models exhibit only a marginal improvement (+2.2 to +6.3) when vision is enabled, even though our benchmark tasks are designed to heavily depend on visual information. By contrast, human performance increases substantially (+22.6) when vision is available, indicating a much stronger dependence on visual input. The limited gains on MLLMs suggest that MLLMs often rely on textual priors rather than truly grounded visual understanding. Overall, these results highlight a fundamental gap between human and model spatial reasoning.

Methods	Avg	RDT	RDR	OL	ADT	DC	ADP	AS
Human [†]	22.6	60.7	23.3	8.8	13.5	16.5	7.9	37.5
Gemini	12.4	15.3	0.9	17.7	16.2	24.3	2.6	7.2
GPT	2.2	-3.3	-1.2	9.3	8.5	-0.2	-13.6	15.1
Qwen3-VL	5.3	5.2	4.1	2.0	8.4	8.2	-10.0	18.7
InternVL3.5	6.3	0.6	1.0	11.2	7.7	-0.3	14.5	7.3
LLaVA-Video	4.9	3.7	4.3	8.1	9.2	-2.4	1.6	9.5
LLaVA-OV	3.3	4.0	11.0	8.0	12.5	-4.0	-1.9	-3.5

Table 3. **Performance gain of vision-enabled over vision-disabled on OpenBench**, evaluated on the largest or latest models within each model family. [†] means evaluated on a tiny subset.



Figure 4. **Performance comparison on VSI-Bench and OpenBench across different sizes and model versions.** We evaluated models from two families, QwenVL and InternVL, each with an older and a newer version. All experiments used inputs of 32 frames for consistency. (a)(b): the overall score of the models across various sizes on the indoor VSI-Bench and OpenBench; lighter colors denote older model versions; the green arrow indicates the performance gain of InternVL3.5-38B over InternVL2-40B. (c): the MRA change on the *absolute distance* task when comparing InternVL3.5 to InternVL2. The green line highlights the performance gain on VSI-Bench, while the red line shows the performance drop on OpenBench. [†]For plotting purposes, models are grouped by their approximate parameter scale. Refer to Sec. F.4 in the supplementary material for detailed results.

Synthetic Abnormal Scenes. To further investigate the extent of linguistic priors, we designed a controlled experiment using two sets of synthetic indoor scenes: a *Normal Set* with conventional object proportions, and an *Abnormal Set* in which object scales were deliberately manipulated while keeping the overall layout unchanged. We generated question–answer pairs for absolute distance and object size estimation on both sets. Results for human evaluators and Gemini-2.5-Pro are shown in Fig. 5.

Gemini performance on both tasks degrades notably when evaluated on the *Abnormal Set*. In contrast, human performance shows only a marginal degradation on these same tasks, indicating that the models’ spatial reasoning is strongly shaped by prior semantic knowledge: their metric estimates collapse when visual evidence contradicts familiar object statistics. More importantly, the drop is highly asymmetric. While accuracy decreases for the *distance* task, the decline is far more severe for the *size* task (e.g., from 54.7 to 28.3 for Gemini). This reflects the fact that size estimation is particularly vulnerable to class-level linguistic priors—models can bypass visual perception and simply output canonical object sizes, a strategy that fails catastrophically in abnormal scenes. The concurrent performance drop in the *distance* task suggests that models also depend on these incorrect size estimates as reference cues for metric reasoning.

4.2. Reasoning with geometric information

To identify the primary bottleneck in metric spatial tasks, we conduct an ablation study in which ground-truth geometric information is progressively revealed to the model. We focus on the *absolute distance* task, which queries the distance between two objects that may not appear in the same frame. The distance d can be calculated by:

$$d = \|(R \cdot p_2 + T) - p_1\|, \quad (1)$$

where p_1 and p_2 are the 3D positions of the two objects in their respective camera coordinate systems at times t_1

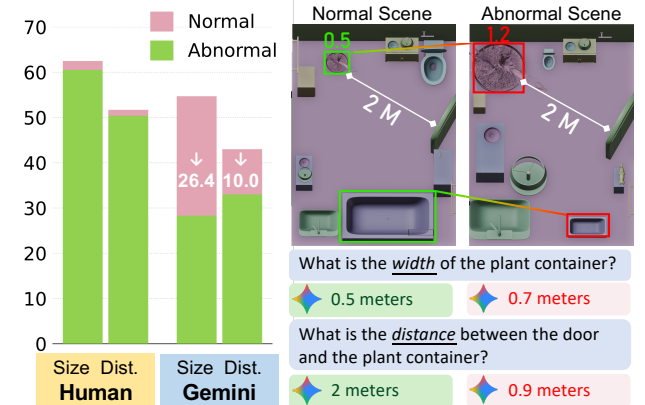


Figure 5. **Illustrations and results of the synthetic test set.** The bar chart (left) shows the performance (\mathcal{MRA}) drop of humans and Gemini-2.5-Pro on the *Size* and *Distance* tasks when evaluated on abnormal scenes versus normal scenes.

and t_2 . The matrix R and the vector T represent the relative camera motion (rotation and translation) from t_1 to t_2 . This formula decomposes the task into two main perceptual components: inferring object positions (p_1, p_2) and inferring camera ego-motion (R, T).

Setting	Qwen3VL-32B	Gemini-2.5-Pro
Vanilla	17.5	19.2
+ One Localization(p_1)	19.2	27.9
+ Both Localization(p_1, p_2)	33.8	40.0
+ Ego-Motion(R, T)	32.5	22.9
+ All(p_1, p_2, R, T)	98.8	98.8
+ All(w/o Formula)	59.2	85.4

Table 4. Ablation study of progressively providing additional geometric information on the absolute distance task.

The results in Tab. 4 reveal several clear trends. First, the **Vanilla** setting performs even worse than in the main benchmark, suggesting that enforcing a structured multi-

step calculation introduces additional parsing complexity that disrupts the model’s default reasoning strategy. Second, both models achieve near-perfect accuracy in the **All** setting, demonstrating that they can execute the mathematical computation without difficulty when all geometric quantities are provided. The sharp contrast between the **All** and **Vanilla** settings confirms that the dominant bottleneck is the extraction of precise metric information from the visual inputs, not the algebraic reasoning itself.

Furthermore, the substantial drop in the **All (w/o Formula)** condition indicates that models do not possess the 3D geometric knowledge required to derive the distance relationship independently—they act as reliable calculators only when explicitly instructed. Finally, although providing partial information (as in the **Both Localization** and **Ego-Motion** settings) yields moderate improvements, performance remains far from ideal, implying that models struggle with both object localization and ego-motion estimation when these components must be inferred visually.

5. Related works

5.1. Multimodal Large Language Models

Multimodal Large Language Models (MLLMs) represent a significant advancement, extending the capabilities of Large Language Models (LLMs) [19, 28, 59] to jointly interpret and synthesize information across heterogeneous modalities [71]. The evolution of MLLMs from foundational methods like CLIP [44] and BLIP-2 [34, 35], to pivotal architectures interfacing visual features with frozen LLMs like Flamingo [2], has led to contemporary systems (e.g., LLaVA [33, 39, 76], Qwen-VL [5], InternVL [14]) that achieve state-of-the-art performance on tasks like VQA [1] and scene understanding [4, 43].

Despite this impressive progress, these foundational MLLMs continue to face significant challenges in visual-spatial reasoning [38]. A strong reliance on textual priors often suppresses fine-grained spatial cues [23]. This issue is exacerbated by the lack of compositional training data specifically designed to foster robust spatial intelligence.

Separate from these foundational models, there is also a growing body of work [10, 15, 16, 24, 62] focused on enhancing specific spatial reasoning capabilities. While these specialized models excel within their designated domains, they typically rely on task-specific training, auxiliary geometric inputs (e.g., depth maps, 3D reconstructions), or explicit region-level supervision. As a result, their capabilities are closely tied to the training distribution and do not reflect the innate spatial understanding of a general-purpose model. Moreover, many such methods are built on static scenes, limiting their ability to reason about motion or dynamic spatial relationships. In contrast, our benchmark evaluates the foundational spatial intelligence of general-purpose MLLMs without introducing new supervision or

additional geometric modalities.

5.2. Benchmarking Spatial Intelligence

Early efforts to evaluate the spatial reasoning abilities of MLLMs primarily focused on reasoning within static single-image scenes, thus assessing qualitative relational understanding [20, 30, 40, 45, 51, 53, 56, 61, 68]. Recently, approaches have evolved to incorporate multi-view images [24, 67, 69] to capture scene complexity and viewpoint changes, or video inputs [25, 65, 77, 78] to evaluate temporal-spatial capabilities.

Beyond qualitative assessment, works like Spatial-RGPT [15] and VSI-Bench [65] began evaluating quantitative measurements in static scenes, based on image and video inputs, respectively. Aiming to reduce linguistic bias, SIRI-Bench [52] uses synthetic videos generated by rendering 3D geometry math problems. Further extending this, STI-Bench [37] introduced the quantitative evaluation of dynamic quantities like speed and displacement.

Nevertheless, the domain imbalance across existing benchmarks remains a major limitation. Most datasets focus on constrained indoor scenes with limited viewpoint diversity and lack coverage of open-world and pedestrian-centric settings. Such bias makes it difficult to assess genuine improvements in spatial reasoning. Moreover, current benchmarks often test recognition and retrieval rather than higher-order reasoning about spatial composition, causality, or physical consistency—key aspects of spatial AI.

6. Conclusion and discussion

Conclusion. We introduced OpenBench, an open-world benchmark for evaluating spatial intelligence in MLLMs across relational, metric, and kinematic reasoning. Built from pedestrian-perspective videos with precise geometric supervision, it enables realistic assessment beyond indoor or synthetic datasets. Our findings expose a structural gap between today’s MLLMs and the level of spatial understanding required for physically grounded AI. They further suggest that scaling visual encoders or expanding training corpora alone is insufficient; genuine progress will require mechanisms capable of inferring, storing, and manipulating 3D geometric quantities in a principled manner.

Discussion. Our ablation studies point toward several promising research avenues. Improving metric depth perception in open-world settings is essential, as this emerges as the principal bottleneck across spatial tasks. Integrating explicit geometric representations—whether through 3D-aware architectures, multi-view consistency, or hybrid symbolic–neural reasoning—may help models move beyond surface-level priors. Moreover, dynamic reasoning remains notably underexplored. Developing models that maintain temporally consistent world models, reason over motion trajectories, and utilize sensor-derived ego-motion data represents a critical next step.

References

[1] Aishwarya Agrawal, Jiasen Lu, Stanislaw Antol, Margaret Mitchell, C. Lawrence Zitnick, Dhruv Batra, and Devi Parikh. Vqa: Visual question answering, 2016. 2, 8

[2] Jean-Baptiste Alayrac, Jeff Donahue, Pauline Luc, Antoine Miech, Iain Barr, Yana Hasson, Karel Lenc, Arthur Mensch, Katherine Millican, Malcolm Reynolds, et al. Flamingo: a visual language model for few-shot learning. *NeurIPS*, 2022. 1, 8

[3] Anthropic. Claude, 2024. 1, 6

[4] Daichi Azuma, Taiki Miyanishi, Shuhei Kurita, and Motoaki Kawanabe. Scanqa: 3d question answering for spatial scene understanding. In *proceedings of the IEEE/CVF conference on computer vision and pattern recognition*, pages 19129–19139, 2022. 8

[5] Jinze Bai, Shuai Bai, Shusheng Yang, Shijie Wang, Sinan Tan, Peng Wang, Junyang Lin, Chang Zhou, and Jingren Zhou. Qwen-vl: A versatile vision-language model for understanding, localization, text reading, and beyond. *arXiv preprint arXiv:2308.12966*, 2023. 8

[6] Shuai Bai, Keqin Chen, Xuejing Liu, Jialin Wang, Wenbin Ge, Sibo Song, Kai Dang, Peng Wang, Shijie Wang, Jun Tang, Humen Zhong, Yuanzhi Zhu, Mingkun Yang, Zhao-hai Li, Jianqiang Wan, Pengfei Wang, Wei Ding, Zheren Fu, Yiheng Xu, Jiabo Ye, Xi Zhang, Tianbao Xie, Zesen Cheng, Hang Zhang, Zhibo Yang, Haiyang Xu, and Junyang Lin. Qwen2.5-vl technical report. *arXiv preprint arXiv:2502.13923*, 2025. 1, 2, 6, 7

[7] Gilad Baruch, Zhuoyuan Chen, Afshin Dehghan, Tal Dimry, Yuri Feigin, Peter Fu, Thomas Gebauer, Brandon Joffe, Daniel Kurz, Arik Schwartz, and Elad Shulman. ARKitscenes - a diverse real-world dataset for 3d indoor scene understanding using mobile RGB-d data. In *NIPS Datasets and Benchmarks Track*, 2021. 2

[8] Gary Bradski. The opencv library. *Dr. Dobb's Journal of Software Tools*, 2000. 1

[9] Holger Caesar, Varun Bankiti, Alex H. Lang, Sourabh Vora, Venice Erin Liang, Qiang Xu, Anush Krishnan, Yu Pan, Giancarlo Baldan, and Oscar Beijbom. nuscenes: A multimodal dataset for autonomous driving. *arXiv preprint arXiv:1903.11027*, 2019. 2

[10] Wenxiao Cai, Iaroslav Ponomarenko, Jianhao Yuan, Xiaoqi Li, Wankou Yang, Hao Dong, and Bo Zhao. Spatialbot: Precise spatial understanding with vision language models. In *2025 IEEE International Conference on Robotics and Automation (ICRA)*, pages 9490–9498, 2025. 2, 8

[11] Carlos Campos, Richard Elvira, Juan J. Gómez, José M. M. Montiel, and Juan D. Tardós. ORB-SLAM3: An accurate open-source library for visual, visual-inertial and multi-map SLAM. *IEEE Transactions on Robotics*, 37(6):1874–1890, 2021. 4, 2, 5

[12] Ming-Fang Chang, John Lambert, Patsorn Sangkloy, Jagjeet Singh, Slawomir Bak, Andrew Hartnett, De Wang, Peter Carr, Simon Lucey, Deva Ramanan, et al. Argoverse: 3d tracking and forecasting with rich maps. In *CVPR*, pages 8748–8757, 2019. 2

[13] Boyuan Chen, Zhuo Xu, Sean Kirmani, Brian Ichter, Dorsa Sadigh, Leonidas Guibas, and Fei Xia. Spatialvlm: Endowing vision-language models with spatial reasoning capabilities. In *CVPR*, pages 14455–14465, 2024. 9

[14] Zhe Chen, Jiannan Wu, Wenhui Wang, Weijie Su, Guo Chen, Sen Xing, Muyan Zhong, Qinglong Zhang, Xizhou Zhu, Lewei Lu, et al. Internvl: Scaling up vision foundation models and aligning for generic visual-linguistic tasks. In *Proceedings of the IEEE/CVF Conference on Computer Vision and Pattern Recognition*, pages 24185–24198, 2024. 1, 8, 6, 7

[15] An-Chieh Cheng, Hongxu Yin, Yang Fu, Qiushan Guo, Ruihan Yang, Jan Kautz, Xiaolong Wang, and Sifei Liu. Spatialrgrpt: Grounded spatial reasoning in vision-language models. In *NIPS*, pages 135062–135093, 2024. 2, 8, 9

[16] An-Chieh Cheng, Yang Fu, Yukang Chen, Zhijian Liu, Xiaolong Li, Subhashree Radhakrishnan, Song Han, Yao Lu, Jan Kautz, Pavlo Molchanov, Hongxu Yin, Xiaolong Wang, and Sifei Liu. 3d aware region prompted vision language model. *arXiv preprint arXiv:2509.13317*, 2025. 8

[17] Angela Dai, Angel X Chang, Manolis Savva, Maciej Halber, Thomas Funkhouser, and Matthias Nießner. Scannet: Richly-annotated 3d reconstructions of indoor scenes. In *CVPR*, pages 5828–5839, 2017. 2

[18] Erik Daxberger, Nina Wenzel, David Griffiths, Haiming Gang, Justin Lazarow, Gefen Kohavi, Kai Kang, Marcin Eichner, Yinfai Yang, Afshin Dehghan, and Peter Grasch. Mm-spatial: Exploring 3d spatial understanding in multimodal llms. *arXiv preprint arXiv:2503.13111*, 2025. 2

[19] DeepSeek-AI. Deepseek-r1: Incentivizing reasoning capability in llms via reinforcement learning, 2025. 8

[20] Zihao Dongfang, Xu Zheng, Ziqiao Weng, Yuanhuiyi Lyu, Danda Pani Paudel, Luc Van Gool, Kailun Yang, and Xuming Hu. Are multimodal large language models ready for omnidirectional spatial reasoning? *arXiv preprint arXiv:2505.11907*, 2025. 8

[21] Haodong Duan, Junming Yang, Yuxuan Qiao, Xinyu Fang, Lin Chen, Yuan Liu, Xiaoyi Dong, Yuhang Zang, Pan Zhang, Jiaqi Wang, et al. Vlmevalkit: An open-source toolkit for evaluating large multi-modality models. In *Proceedings of the 32nd ACM International Conference on Multimedia*, pages 11198–11201, 2024. 4, 5

[22] Mark Everingham, Luc Van Gool, Christopher KI Williams, John Winn, and Andrew Zisserman. The pascal visual object classes (voc) challenge. *International journal of computer vision*, 88(2):303–338, 2010. 5

[23] Aarti Ghatkesar, Uddesha Upadhyay, and Ganesh Venkatesh. Looking beyond language priors: Enhancing visual comprehension and attention in multimodal models. *arXiv preprint arXiv:2505.05626*, 2025. 8

[24] Mohsen Gholami, Ahmad Rezaei, Zhou Weimin, Sitong Mao, Shunbo Zhou, Yong Zhang, and Mohammad Akbari. Spatial reasoning with vision-language models in ego-centric multi-view scenes, 2025. 2, 8, 4

[25] Ziyang Gong, Wenhao Li, Oliver Ma, Songyuan Li, Zhaokai Wang, Songyuan Li, Jiayi Ji, Xue Yang, Gen Luo, Junchi Yan, and Rongrong Ji. Space-10: A comprehensive bench-

mark for multimodal large language models in compositional spatial intelligence, 2025. 2, 8

[26] Dong Guo et al. Seed1.5-vl technical report, 2025. 1, 6

[27] Richard Hartley and Andrew Zisserman. *Multiple View Geometry in Computer Vision*. Cambridge University Press, Cambridge, UK, 2 edition, 2004. 2

[28] Aaron Hurst, Adam Lerer, Adam P Goucher, Adam Perelman, Aditya Ramesh, Aidan Clark, AJ Ostrow, Akila Welihinda, Alan Hayes, Alec Radford, et al. Gpt-4o system card. *arXiv preprint arXiv:2410.21276*, 2024. 1, 8, 6

[29] Mengdi Jia, Zekun Qi, Shaochen Zhang, Wenyao Zhang, Xinjiang Yu, Jiawei He, He Wang, and Li Yi. Omnispatial: Towards comprehensive spatial reasoning benchmark for vision language models, 2025. 2

[30] Justin Johnson, Bharath Hariharan, Laurens Van Der Maaten, Li Fei-Fei, C Lawrence Zitnick, and Ross Girshick. Clevr: A diagnostic dataset for compositional language and elementary visual reasoning. In *CVPR*, 2017. 8

[31] Nikita Karaev, Iurii Makarov, Jianyuan Wang, Natalia Neverova, Andrea Vedaldi, and Christian Rupprecht. Co-Tracker3: Simpler and better point tracking by pseudo-labelling real videos. 2024. 4, 3

[32] Alexander Kirillov, Eric Mintun, Nikhila Ravi, Hanzi Mao, Chloe Rolland, Laura Gustafson, Tete Xiao, Spencer Whitehead, Alexander C. Berg, Wan-Yen Lo, Piotr Dollár, and Ross Girshick. Segment anything. *arXiv:2304.02643*, 2023. 3

[33] Bo Li, Yuanhan Zhang, Dong Guo, Renrui Zhang, Feng Li, Hao Zhang, Kaichen Zhang, Yanwei Li, Ziwei Liu, and Chunyuan Li. Llava-onevision: Easy visual task transfer. *arXiv preprint arXiv:2408.03326*, 2024. 1, 8, 6

[34] Junnan Li, Dongxu Li, Caiming Xiong, and Steven Hoi. BLIP: Bootstrapping language-image pre-training for unified vision-language understanding and generation. In *ICML*. PMLR, 2022. 8

[35] Junnan Li, Dongxu Li, Silvio Savarese, and Steven Hoi. BLIP-2: Bootstrapping language-image pre-training with frozen image encoders and large language models. In *ICML*. PMLR, 2023. 8

[36] Qixiu Li, Yaobo Liang, Zeyu Wang, Lin Luo, Xi Chen, Mozheng Liao, Fangyun Wei, Yu Deng, Sicheng Xu, Yizhong Zhang, et al. Cogact: A foundational vision-language-action model for synergizing cognition and action in robotic manipulation. *arXiv preprint arXiv:2411.19650*, 2024. 2

[37] Yun Li, Yiming Zhang, Tao Lin, Xiangrui Liu, Wenxiao Cai, Zheng Liu, and Bo Zhao. Sti-bench: Are mllms ready for precise spatial-temporal world understanding?, 2025. 2, 3, 8, 4

[38] Fangyu Liu, Guy Emerson, and Nigel Collier. Visual spatial reasoning. *Transactions of the Association for Computational Linguistics*, 11:635–651, 2023. 8

[39] Haotian Liu, Chunyuan Li, Yuheng Li, Bo Li, Yuanhan Zhang, Sheng Shen, and Yong Jae Lee. Llava-next: Improved reasoning, ocr, and world knowledge, 2024. 8

[40] Jingping Liu, Ziyan Liu, Zhedong Cen, Yan Zhou, Yinan Zou, Weiyang Zhang, Haiyun Jiang, and Tong Ruan. Can multimodal large language models understand spatial relations? *arXiv preprint arXiv:2505.19015*, 2025. 8

[41] Shilong Liu, Zhaoyang Zeng, Tianhe Ren, Feng Li, Hao Zhang, Jie Yang, Chunyuan Li, Jianwei Yang, Hang Su, Jun Zhu, et al. Grounding dino: Marrying dino with grounded pre-training for open-set object detection. *arXiv preprint arXiv:2303.05499*, 2023. 3

[42] Shiyin Lu, Yang Li, Qing-Guo Chen, Zhao Xu, Weihua Luo, Kaifu Zhang, and Han-Jia Ye. Ovis: Structural embedding alignment for multimodal large language model. *arXiv preprint arXiv:2405.20797*, 2024. 1, 6

[43] Bryan A Plummer, Liwei Wang, Chris M Cervantes, Juan C Caicedo, Julia Hockenmaier, and Svetlana Lazebnik. Flickr30k entities: Collecting region-to-phrase correspondences for richer image-to-sentence models. In *Proceedings of the IEEE international conference on computer vision*, pages 2641–2649, 2015. 2, 8

[44] Alec Radford, Jong Wook Kim, Chris Hallacy, Aditya Ramesh, Gabriel Goh, Sandhini Agarwal, Girish Sastry, Amanda Askell, Pamela Mishkin, Jack Clark, et al. Learning transferable visual models from natural language supervision. In *ICML*. PMLR, 2021. 1, 8

[45] Santhosh Kumar Ramakrishnan, Erik Wijmans, Philipp Kraehenbuehl, and Vladlen Koltun. Does spatial cognition emerge in frontier models? In *The Thirteenth International Conference on Learning Representations*, 2025. 8

[46] Nikhila Ravi, Valentin Gabeur, Yuan-Ting Hu, Ronghang Hu, Chaitanya Ryali, Tengyu Ma, Haitham Khedr, Roman Rädle, Chloe Rolland, Laura Gustafson, Eric Mintun, Junting Pan, Kalyan Vasudev Alwala, Nicolas Carion, Chao-Yuan Wu, Ross Girshick, Piotr Dollár, and Christoph Feichtenhofer. Sam 2: Segment anything in images and videos, 2024. 3

[47] Joern Rehder, Janosch Nikolic, Thomas Schneider, Timo Hinzmann, and Roland Siegwart. Extending kalibr: Calibrating the extrinsics of multiple imus and of individual axes. In *2016 IEEE international conference on robotics and automation (ICRA)*, pages 4304–4311. IEEE, 2016. 1

[48] Tianhe Ren, Shilong Liu, Ailing Zeng, Jing Lin, Kun-chang Li, He Cao, Jiayu Chen, Xinyu Huang, Yukang Chen, Feng Yan, Zhaoyang Zeng, Hao Zhang, Feng Li, Jie Yang, Hongyang Li, Qing Jiang, and Lei Zhang. Grounded sam: Assembling open-world models for diverse visual tasks, 2024. 2

[49] Johannes Lutz Schönberger and Jan-Michael Frahm. Structure-from-motion revisited. In *CVPR*, 2016. 2

[50] Johannes Lutz Schönberger, Enliang Zheng, Marc Pollefeys, and Jan-Michael Frahm. Pixelwise view selection for unstructured multi-view stereo. In *ECCV*, 2016. 2

[51] Fatemeh Shiri, Xiao-Yu Guo, Mona Far, Xin Yu, Reza Haf, and Yuan-Fang Li. An empirical analysis on spatial reasoning capabilities of large multimodal models. In *Proceedings of the 2024 Conference on Empirical Methods in Natural Language Processing*, pages 21440–21455, 2024. 8

[52] Zijian Song, Xiaoxin Lin, Qiuming Huang, Guangrun Wang, and Liang Lin. Siri-bench: Challenging vlm's spatial in-

telligence through complex reasoning tasks. *arXiv preprint arXiv:2506.14512*, 2025. 8

[53] Ilias Stogiannidis, Steven McDonagh, and Sotirios A Tsaftaris. Mind the gap: Benchmarking spatial reasoning in vision-language models. *arXiv preprint arXiv:2503.19707*, 2025. 8

[54] Pei Sun, Henrik Kretzschmar, Xerxes Dotiwalla, Aurelien Chouard, Vijaysai Patnaik, Paul Tsui, James Guo, Yin Zhou, Yuning Chai, Benjamin Caine, et al. Scalability in perception for autonomous driving: Waymo open dataset. In *CVPR*, pages 2446–2454, 2020. 2

[55] Andrew Szot, Bogdan Mazoure, Omar Attia, Aleksei Timofeev, Harsh Agrawal, Devon Hjelm, Zhe Gan, Zsolt Kira, and Alexander Toshev. From multimodal llms to generalist embodied agents: Methods and lessons. In *Proceedings of the IEEE/CVF Conference on Computer Vision and Pattern Recognition (CVPR)*, pages 10644–10655, 2025. 2

[56] Yihong Tang, Ao Qu, Zhaokai Wang, Dingyi Zhuang, Zhaofeng Wu, Wei Ma, Shenhao Wang, Yunhan Zheng, Zhan Zhao, and Jinhua Zhao. Sparkle: Mastering basic spatial capabilities in vision language models elicits generalization to spatial reasoning. *arXiv preprint arXiv:2410.16162*, 2024. 8

[57] Gemini Team, Rohan Anil, Sebastian Borgeaud, Jean-Baptiste Alayrac, Jiahui Yu, Radu Soricut, Johan Schalkwyk, Andrew M Dai, Anja Hauth, Katie Millican, et al. Gemini: a family of highly capable multimodal models. *arXiv preprint arXiv:2312.11805*, 2023. 1, 3, 6

[58] Qwen Team. Qwen3-vl: The multimodal large language model series. <https://github.com/QwenLM/Qwen3-VL>, 2025. 1, 6

[59] Hugo Touvron, Thibaut Lavril, Gautier Izacard, Xavier Martinet, Marie-Anne Lachaux, Timothée Lacroix, Baptiste Rozière, Naman Goyal, Eric Hambro, Faisal Azhar, Aurelien Rodriguez, Armand Joulin, Edouard Grave, and Guillaume Lample. Llama: Open and efficient foundation language models, 2023. 8

[60] Weiyun Wang et al. Internvl3.5: Advancing open-source multimodal models in versatility, reasoning, and efficiency, 2025. 1, 6

[61] Xingrui Wang, Wufei Ma, Tiezheng Zhang, Celso M de Melo, Jieneng Chen, and Alan Yuille. Spatial457: A diagnostic benchmark for 6d spatial reasoning of large multimodal models. In *CVPR*, 2025. 8

[62] Zhaozhi Wang, Tong Zhang, Mingyue Guo, Yaowei Wang, and Qixiang Ye. Videoanchor: Reinforcing subspace-structured visual cues for coherent visual-spatial reasoning, 2025. 8

[63] Yanhao Wu, Haoyang Zhang, Tianwei Lin, Lichao Huang, Shujie Luo, Rui Wu, Congpei Qiu, Wei Ke, and Tong Zhang. Generating multimodal driving scenes via next-scene prediction. In *Proceedings of the Computer Vision and Pattern Recognition Conference*, pages 6844–6853, 2025. 2

[64] Guohang Yan, Zhuochun Liu, Chengjie Wang, Chunlei Shi, Pengjin Wei, Xinyu Cai, Tao Ma, Zhizheng Liu, Zebin Zhong, Yuqian Liu, Ming Zhao, Zheng Ma, and Yikang Li. Opencalib: A multi-sensor calibration toolbox for autonomous driving. *arXiv preprint arXiv:2205.14087*, 2022. 1, 2

[65] Jihan Yang, Shusheng Yang, Anjali W Gupta, Rilyn Han, Li Fei-Fei, and Saining Xie. Thinking in space: How multimodal large language models see, remember, and recall spaces. In *CVPR*, pages 10632–10643, 2025. 1, 2, 3, 5, 6, 8, 4, 7, 9

[66] Lihe Yang, Bingyi Kang, Zilong Huang, Zhen Zhao, Xiaogang Xu, Jiashi Feng, and Hengshuang Zhao. Depth anything v2. *arXiv:2406.09414*, 2024. 2

[67] Sihan Yang, Runsen Xu, Yiman Xie, Sizhe Yang, Mo Li, Jingli Lin, Chenming Zhu, Xiaochen Chen, Haodong Duan, Xiangyu Yue, Dahua Lin, Tai Wang, and Jiangmiao Pang. Mmsi-bench: A benchmark for multi-image spatial intelligence. *arXiv preprint arXiv:2505.23764*, 2025. 2, 8

[68] Ruilin Yao, Bo Zhang, Jirui Huang, Xinwei Long, Yifang Zhang, Tianyu Zou, Yufei Wu, Shichao Su, Yifan Xu, Wenxi Zeng, Zhaoyu Yang, Guoyou Li, Shilan Zhang, Zichan Li, Yaxiong Chen, Shengwu Xiong, Peng Xu, Jiajun Zhang, Bowen Zhou, David Clifton, and Luc Van Gool. Lens: Multi-level evaluation of multimodal reasoning with large language models, 2025. 8

[69] Chun-Hsiao Yeh, Chenyu Wang, Shengbang Tong, Ta-Ying Cheng, Ruoyu Wang, Tianzhe Chu, Yuexiang Zhai, Yubei Chen, Shenghua Gao, and Yi Ma. Seeing from another perspective: Evaluating multi-view understanding in mllms, 2025. 2, 5, 8, 9

[70] Chandan Yeshwanth, Yueh-Cheng Liu, Matthias Nießner, and Angela Dai. Scannet++: A high-fidelity dataset of 3d indoor scenes. In *CVPR*, pages 12–22, 2023. 2

[71] Shukang Yin, Chaoyou Fu, Sirui Zhao, Ke Li, Xing Sun, Tong Xu, and Enhong Chen. A survey on multimodal large language models. *National Science Review*, 11(12), 2024. 8

[72] Jiayao Zhang, Weiyao Huang, Bo Peng, Mingdong Wu, Fei Hu, Zijian Chen, Bo Zhao, and Hao Dong. Omni6dpose: A benchmark and model for universal 6d object pose estimation and tracking, 2024. 2

[73] Jiahui Zhang, Yurui Chen, Yanpeng Zhou, Yueming Xu, Ze Huang, Jilin Mei, Junhui Chen, Yu-Jie Yuan, Xinyue Cai, Guowei Huang, Xingyue Quan, Hang Xu, and Li Zhang. From flatland to space: Teaching vision-language models to perceive and reason in 3d, 2025. 2

[74] Weichen Zhang, Zile Zhou, Xin Zeng, Liu Xuchen, Jianjie Fang, Chen Gao, Jinqiang Cui, Yong Li, Xinlei Chen, and Xiao-Ping Zhang. Open3d-vqa: A benchmark for embodied spatial concept reasoning with multimodal large language model in open space. In *Proceedings of the 33rd ACM International Conference on Multimedia*, pages 12784–12791, 2025. 2

[75] Youcui Zhang, Xinyu Huang, Jinyu Ma, Zhaoyang Li, Zhaochuan Luo, Yanchun Xie, Yuzhuo Qin, Tong Luo, Yaqian Li, Shilong Liu, et al. Recognize anything: A strong image tagging model. *arXiv preprint arXiv:2306.03514*, 2023. 2

[76] Yuanhan Zhang, Bo Li, haotian Liu, Yong jae Lee, Liangke Gui, Di Fu, Jiashi Feng, Ziwei Liu, and Chunyuan Li. Llava-next: A strong zero-shot video understanding model, 2024. 1, 8, 6

- [77] Zheyuan Zhang, Fengyuan Hu, Jayjun Lee, Freda Shi, Parisa Kordjamshidi, Joyce Chai, and Ziqiao Ma. Do vision-language models represent space and how? evaluating spatial frame of reference under ambiguities. In *ICLR*, 2025. [8](#)
- [78] Shijie Zhou, Alexander Vilesov, Xuehai He, Ziyu Wan, Shuwang Zhang, Aditya Nagachandra, Di Chang, Dongdong Chen, Xin Eric Wang, and Achuta Kadambi. Vlm4d: Towards spatiotemporal awareness in vision language models, 2025. [8](#)

From Indoor to Open World: Revealing the Spatial Reasoning Gap in MLLMs

Supplementary Material

Appendix Outline

In the supplementary material, we provide:

- Visual illustration of linguistic priors;
- Technical details of data collection and benchmark construction;
- Error analysis and pipeline validation;
- Evaluation setups and experiment details;
- More evaluation results.
- Privacy statement.

A. Illustration of Linguistic Priors

To clearly demonstrate that models rely on **linguistic priors** when answering spatial questions, and that this reliance can lead to wrong answers, we use a scene from a miniature room to ask models about size questions, as illustrated in Fig. 6.

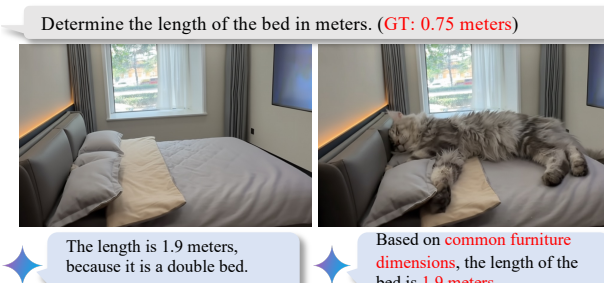


Figure 6. **Illustration of a Prior-Driven Reasoning Failure.** The scene is a 1:3 scale miniature bed. (**Left**) Gemini-2.5-Pro defaults to its internal knowledge, identifying the object as a “double bed” and outputting a prior-based estimate of 1.9m. (**Right**) Even when a strong, contradictory visual clue (a real cat) is introduced, the model fails to ground its reasoning in the visual evidence, and still defaults to the same “common furniture dimension” prior and outputs 1.9m.

B. Details of Data Collection

B.1. Hardware Specifications

Our custom-built data collection platform, illustrated in the main paper, is equipped with a multi-sensor suite designed for high-fidelity, pedestrian-centric data capture. The core components include:

- A synchronized stereo RGB camera system (rolling shutter, 1080p, 15 FPS).
- A 32-beam omnidirectional LiDAR (10 FPS).
- A high-frequency Inertial Measurement Unit (IMU) operating at 100 Hz.

- A GPS unit operating at 1 Hz.

All sensors are connected to an onboard Intel NUC mini PC running Ubuntu, which is orchestrated by the widely-adopted ROS2 framework. This system provides unified, single-command control over the entire sensor suite and logs all multimodal data streams as timestamp-synchronized ROS2 bag files, facilitating robust subsequent extraction and processing. The entire platform is powered by an onboard battery, which provides approximately one hour of continuous operation per charge.

To ensure smooth motion capture, the platform was mounted on a manual cart. The camera system was positioned at approximately 1.4 meters from the ground. This height was deliberately chosen as a trade-off to balance the need for a pedestrian-like perspective with the critical requirement of maintaining motion stability during collection.

B.2. Calibration and Rectification

A rigorous multi-sensor calibration pipeline was executed prior to all data processing to ensure the metric accuracy and spatio-temporal alignment of our dataset. This process was divided into three main components:

Stereo Camera Calibration and Rectification. We first calibrated the stereo camera system. This process involved using a standard chessboard pattern with the OpenCV library [8] to precisely determine the intrinsic parameters of each camera and the extrinsic transformation between the left and right camera units. Following calibration, a stereo rectification algorithm, also from OpenCV, was applied to all image pairs. This step is critical as it warps the two images such that their epipolar lines become collinear and horizontal, which allows for subsequent stereo matching and SLAM tasks. All visual data used in the downstream modules of our pipeline consists of these rectified stereo images.

LiDAR-to-Camera Calibration. To fuse visual and depth information, we calibrated the extrinsic parameters (the 6-DoF transformation) between the LiDAR and the left camera of the stereo system. This calibration was performed using the OpenCalib ToolBox [64], which provides robust automatic calibration. The resulting transformation matrix is essential for our pipeline, as it allows us to accurately project the 3D LiDAR point clouds onto the 2D image plane of the camera to generate the metric-scale sparse depth maps.

IMU Calibration. Finally, the Inertial Measurement Unit (IMU) was calibrated in two stages. We first determined its intrinsic parameters using the Kalibr toolbox [47]. Subsequently, the extrinsic transformation between the IMU and

the stereo camera system was computed using the OpenCalib ToolBox [64]. This precise IMU-camera extrinsic calibration is a prerequisite for ensuring the accuracy and robustness of the stereo-inertial SLAM module used for camera pose estimation.

B.3. Operators and Scene Selection

Operators were instructed to navigate the cart through the selected scenes at a typical walking speed. Turns were intentionally included in the routes to better represent natural pedestrian movement and to generate diverse trajectories for the final evaluation tasks. The entire data collection process totaled over 100 person-hours.

As referenced in the main paper, our scene selection strategy focused on maximizing diversity while capturing typical environments a pedestrian encounters. Furthermore, other than outdoor scenes, we include large-scale shopping malls to incorporate complex indoor scenarios. Unlike the confined residential or office environments common in existing benchmarks, large malls feature open layouts and a significantly larger range of scales, presenting open-world spatial challenges. Representative samples of our chosen scenes are shown in Fig. 7. We recognize that open-world environments can be more spacious and semantically sparse compared to object-dense indoor scenes. Therefore, our collection protocol intentionally prioritized pedestrian-centric areas known for a high density of potential query targets (e.g., street furniture, signage, complex storefronts, and other pedestrians) to ensure the final benchmark is both diverse and challenging.

Following a manual curation process, where we discarded sequences with poor visual quality (e.g., blur, low light) or those lacking distinct queryable objects, we obtained a 20-hour high-quality multimodal dataset. While approximately 6 hours of this data were used for the benchmark construction detailed in this paper, the remaining dataset, including all raw sensor data, will be made publicly available to the research community to foster further development in spatial intelligence.

C. Details for OpenBench construction

Video Segmentation and Synchronization. For processing efficiency, we segment the long-form raw recordings **logically** rather than physically. Instead of duplicating or moving source data, each clip is defined by a JSON file that bundles all necessary, timestamp-synchronized metadata, including paths to the stereo image frames, LiDAR PCD files, and IMU/GPS data. These logical clips are defined with randomized durations between 15 to 30 seconds. This duration, shorter than those commonly used in indoor datasets [17], is a deliberate design choice for two reasons: (1) the high semantic density of open-world scenes ensures sufficient complexity, comparable to much longer indoor

recordings; and (2) it aligns with the sparse-frame sampling approach inherent to video loading for most MLLMs, ensuring effective capture of dynamic events.

Camera Pose Estimation. We employ ORB-SLAM3 [11] in its stereo-inertial mode, which utilizes our rectified 15 FPS stereo image sequences and IMU data. We found that processing the original full-resolution (1080p) frames was unreliable for this algorithm. Therefore, all input images were first downsampled to 960x540, and their corresponding camera intrinsic parameters were rescaled accordingly. This process yields a precise, metric-scale pose in a world coordinate system for every frame. This method was selected after an empirical evaluation on our data, where it demonstrated superior robustness and accuracy compared to the classical SfM pipeline COLMAP [49, 50].

Densified Depth Map Generation. To address the inherent sparsity of single-frame LiDAR scans, we leverage the estimated camera poses to perform multi-frame point cloud fusion. For each frame, point clouds from temporally adjacent frames are transformed and aggregated according to their relative poses, yielding a denser fused point cloud. This fused representation is then projected onto the image plane—following the projection protocol described earlier—to produce a densified depth map. These enhanced depth maps are essential for accurate downstream 3D information extraction. In our final implementation, we set the temporal fusion window to 3, meaning the point cloud for each frame is aggregated with those of its immediately preceding and succeeding frames.

Keyframe Selection. We extract keyframes from each video clip at a fixed 30-frame interval. This sampling rate (equivalent to 2 seconds at 15 FPS) was chosen to strike a balance: it is frequent enough to capture the vast majority of objects appearing in the pedestrian-speed video, yet sparse enough to avoid redundant annotation efforts on highly similar, consecutive frames.

Captioning with MLLMs. For captioning objects in the keyframes, our initial approach adopted the pipeline from GroundedSAM [48], using an open-vocabulary tagging model [75] to generate candidate class names. However, we observed that for our pedestrian-centric, open-world scenes, these models exhibit a strong bias towards labeling large, semantically dominant regions. This resulted in a high density of unsuitable, non-object labels such as ‘road’, ‘sky’, or ‘buildings’, which are ill-suited as query targets for a spatial benchmark. Thus, we choose to instruct a locally-run MLLM, Qwen-2.5-VL-8B-Instruct [6] to identify multiple semantically clear, physically distinct objects in each keyframe. For each object, the model generates a detailed caption describing only its intrinsic properties (e.g., ‘a red fire hydrant’) and classifies it as either static or dynamic. This yields high-quality, relevant textual descriptions for subsequent grounding. See Fig. 8 for the prompt used in

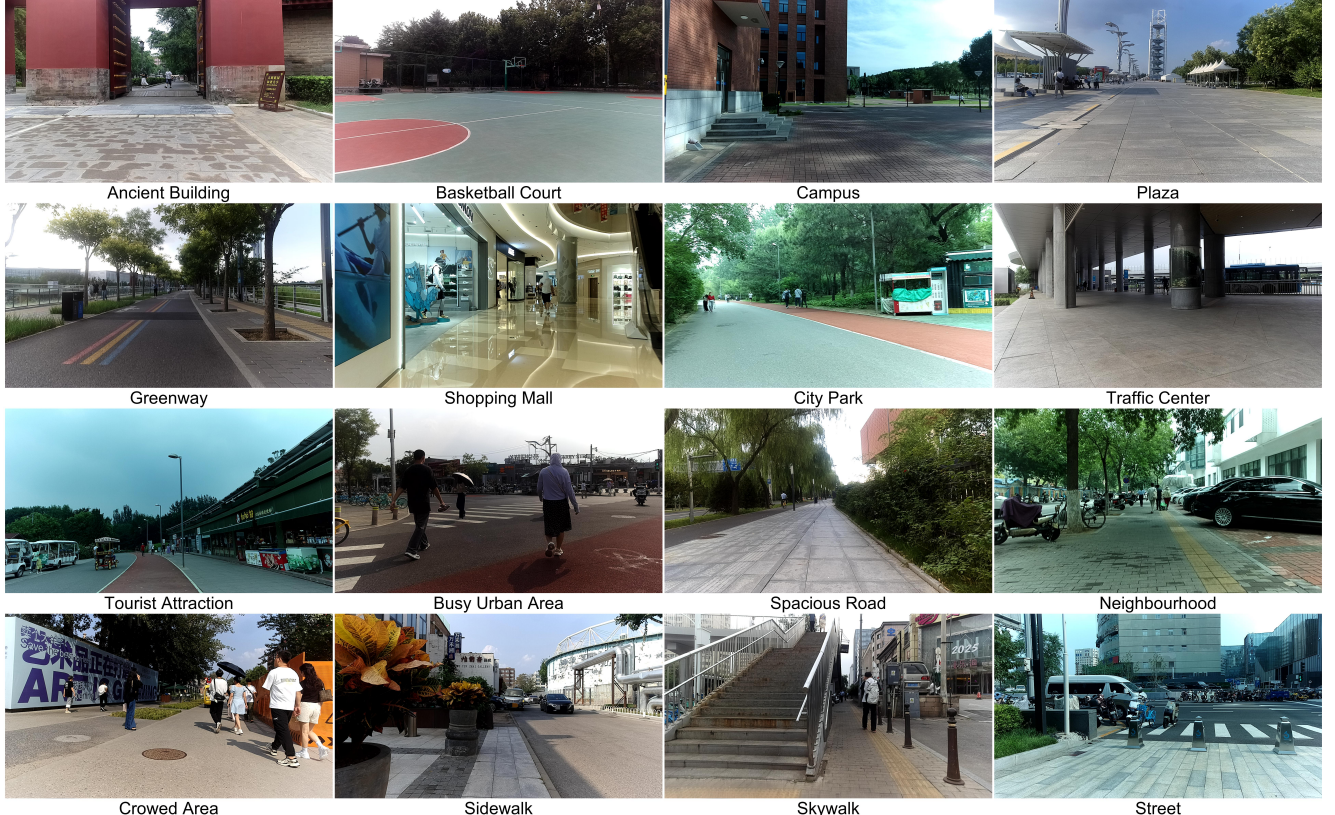


Figure 7. Representative Samples of Scenes in OpenBench.

this phase.

Object Detection and Segmentation. The object captions generated in the previous step serve as text prompts for GroundingDINO [41] to produce 2D bounding boxes. These boxes are then refined into pixel-level segmentation masks by the SAM model [32]. As each caption corresponds to a single object instance, we select only the highest-confidence detection per caption, followed by Non-Maximum Suppression (NMS) to resolve potential part-whole ambiguities.

Temporal Object Tracking. To ensure robust temporal consistency, we employ a point-tracking paradigm over a mask-propagation approach. While recent segmentation models like SAM2 [46] offer tracking, their propagation-based method can lead to drift and errors in long-term tracking. We use a point tracking model (CoTracker3 [31]) to establish motion correspondence. We sample points within an object’s keyframe mask, track them bidirectionally, and then use these tracked points on non-key frames with SAM to generate a final, temporally coherent mask sequence.

3D Spatial Registration. To obtain each object’s 3D representation, we use the per-frame mask to extract the corresponding depth values from the depth map. These values are then used to deproject the masked pixels into a 3D point

cloud, whose centroid serves as the object’s estimated 3D position relative to the camera. By combining this relative position with the frame’s global camera pose, we register all objects into a unified world coordinate system. We note that as our LiDAR data primarily captures the front-facing surfaces of objects, we do not provide estimations of their full 3D dimensions (width, height, depth) in the current version of the benchmark. A final de-duplication step is performed in this world space to merge instances of the same static object detected in different keyframes.

See Fig. 16 for detailed samples illustrating the Joint-Annotation Module’s workflow.

Template-based Generation. We use a template-based approach to generate all question-answer pairs in order to separate and test the models’ spatial reasoning capabilities, minimizing the influence of complex language understanding or multi-step logical reasoning as confounding variables. The full templates for 9 tasks are shown in Tab. 5.

MLLM-assisted Curation. First, a powerful closed-source MLLM (e.g., Gemini-2.5-Pro [57]) performs an initial pass to correct inaccurate captions and filter out questions related to objects that are poorly visible due to occlusion or detection errors. Second, the MLLM assigns a confidence score to the remaining QA pairs, flagging those with potential am-

Captioner Prompt

[Task]

Your task is to analyze an image and output a JSON object containing lists of captions for static and dynamic objects.

[Rules]

1. Content Principle: Identify distinct physical objects. Each string in the lists must describe a **single entity**. Avoid plural or group descriptions (e.g., instead of “cars”, list “blue sedan”, “white SUV”).
2. Ignore: Backgrounds (walls, roads), 2D elements (text, signs), minor parts of larger objects, natural or amorphous categories like “tree”, “bush”, “flowers”, “grass”, or “cloud”.
3. Uniqueness: If an object has already been listed, do not list it again. Once no new unique objects can be found, STOP immediately and close the JSON list with a bracket.
4. Classification: The identified objects should first be classified into static or dynamic.
static objects: Stationary items. (e.g., a parked car, a bench, a trash bin).
dynamic objects: Items visibly in motion. (e.g., a person walking, a car driving, a bird flying).
5. Captions: All captions must be purely visual descriptions (e.g., “red sports car”, “person in yellow jacket”). Do not describe motion (e.g., avoid “person walking”).
6. Empty Lists: If no objects of a certain type are found, use an empty list “[]”.

[Example]

```
{  
  "static_objects": [  
    "red sports car",  
    "black street lamp",  
    "green park bench"  
  ],  
  "dynamic_objects": [  
    "man in blue jacket"  
  ]  
}
```

Your entire response must be a single, valid JSON object, strictly following the format shown in the ‘[example]’. Do not add any other text.

Figure 8. Prompt for the MLLM captioner.

biguities or unstable visual tags. Finally, human annotators conduct a final review of all low-confidence samples, either correcting or discarding them.

See Fig. 13, Fig. 14 and Fig. 15 for more examples in OpenBench.

D. Error Analysis of Benchmark Construction

Unlike benchmarks built upon existing, manually annotated 3D datasets [24, 37, 65], OpenBench employs a highly automated pipeline to extract spatial information and generate QA pairs. While this automation enables scalability, it is crucial to analyze the potential sources of error. In this section, we analyze these errors and demonstrate that they are minimal, and that the quality of OpenBench is ensured through our rigorous calibration, validation, and curation processes.

Three primary aspects could introduce errors into the final ground truth answers: (i) the extrinsic and intrinsic calibration of the sensors, (ii) the pose estimation from the SLAM algorithm, and (iii) the final 3D registration of objects in the world coordinate.

D.1. Errors in Calibrations

To ensure data fidelity, we conducted several independent calibration processes for all sensors and selected the optimal results. The quality of the stereo calibration can be measured by its *reprojection error*, which quantifies the distance between a detected pattern keypoint and its corresponding point projected from the other camera view. Using a standard chessboard pattern, our final selected calibration (from 25 image pairs) achieved a mean reprojection error of **0.32 pixels**.

Task	Question Template
Relative Distance	Measuring from the closest point of each object, which of the following is closest to the $\{Q_class\}(id:\{Q_id\})$: $\{A_class\}(id:\{A_id\})$, $\{B_class\}(id:\{B_id\})$, $\{C_class\}(id:\{C_id\})$, or $\{D_class\}(id:\{D_id\})$?
Relative Direction	If I am standing by the $\{C_class\}(id:\{C_id\})$ and facing the $\{A_class\}(id:\{A_id\})$, is the $\{B_class\}(id:\{B_id\})$ to my front-left, front-right, back-left, or back-right? The directions refer to the quadrants of a Cartesian plane.
Qualitative Ego-Motion	Assuming the video is recorded from a first-person perspective, which of the provided options best describes the person's overall movement throughout the entire duration of the video? Choose from straight, left turn, right turn or U turn.
Object 3D Localization	At approximately $\{T\}$ seconds into the video, what is the Euclidean distance of the $\{A_class\}(id:\{A_id\})$ from the camera in meters?
Absolute Distance	What's the distance between the center of the $\{A_class\}(id:\{A_id\})$ and the $\{B_class\}(id:\{B_id\})$ in meters?
Depth-aware Counting	At approximately $\{time_sec\}$ s, how many $\{class_name\}$ s are visible within $\{distance_threshold\}$ meters from the camera?
Absolute Displacement	What is the displacement distance of the $\{A_class\}(id:\{A_id\})$ between $\{T1\}$ s and $\{T2\}$ s in meters?
Absolute Speed	What is the average speed of the $\{A_class\}(id:\{A_id\})$ between $\{T1\}$ s and $\{T2\}$ s in m/s?
Quantitative Ego-Motion	How long has the camera travelled throughout the entire duration of the video in meters?

Table 5. Templates used for question-answer pairs generation.

Similarly, the LiDAR-to-camera calibration quality was measured by the reprojection error between 3D LiDAR points and their corresponding 2D image keypoints. Using 25 pairs, the mean reprojection error was **0.51 pixels**. We further validated this by measuring the planarity error between the checkerboard plane in the LiDAR point cloud and in the camera view. The mean translation error was **0.002 meters** and the mean rotation error was **0.978 degrees**, indicating a highly accurate spatial alignment between the sensors.

D.2. Errors in SLAM Pose Estimation

A quantitative evaluation of the final pose accuracy from ORB-SLAM3 [11] on our dataset is not feasible due to the lack of ground-truth trajectories in our collection. Instead, we rely on the extensive public validation of the algorithm itself. The original ORB-SLAM3 paper, for example, reports an Absolute Trajectory Error (ATE) of **0.035 meters** on comparable stereo-inertial datasets, demonstrating its high metric precision.

D.3. Errors in World 3D Registration

Several potential error sources could introduce error to the final 3D registration of semantic objects. These include visual occlusions, imperfect segmentation masks, minor tem-

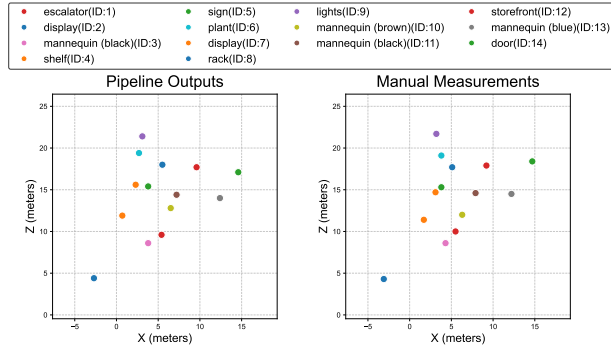
poral misalignments between the keyframe and the fused depth map, and the approximation of an object's center using its visible point cloud centroid.

To provide a qualitative validation of the pipeline's end-to-end accuracy, we conducted a real-world verification. We conducted this verification in two representative scenes: an indoor mall and an outdoor campus. For each scene, we first generated a 2D map of all static objects using our full pipeline. Subsequently, we returned to the physical locations to create a corresponding reference map by manually measuring the same objects' relative positions. As visualized in Fig. 9, the comparison reveals a low mean positional error between the pipeline output and the manual ground truth: 0.68 meters for the indoor scene and 0.79 meters for the outdoor scene, respectively. This result confirms the high metric fidelity of our automated generation pipeline.

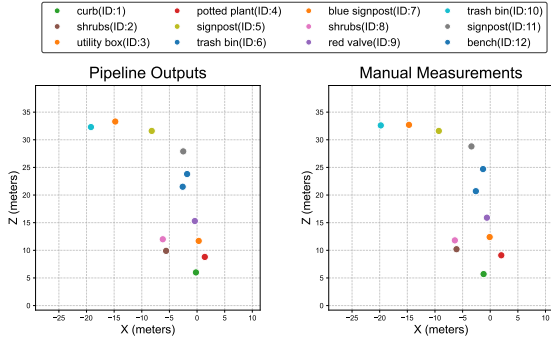
E. Evaluation Details

E.1. General Evaluation Setup

All evaluations are conducted using the VLMEvalKit framework [21] to ensure a standardized protocol, running on NVIDIA RTX 4090 GPUs. Unless specified otherwise, we employ a greedy decoding strategy (i.e., temperature=0, top-k=1, top-p=1) for all models to ensure reproducibility.



(a) Validation of our pipeline in an indoor mall scene.



(b) Validation of our pipeline in an outdoor campus scene.

Figure 9. Qualitative Validation of the Pipeline. We compare the map of static objects generated by our automated pipeline (left) against a ground-truth map of the same scene, which was measured manually on-site (right). The two maps are aligned for comparison.

For closed-source models, we evaluate Gemini-2.5-Pro, Gemini-2.5-Flash [57], GPT-5, GPT-4o [28], Claude-3.7-Sonnet, Claude-4-Sonnet [3], Doubao-Seed-Vision [26]. For open-source models, we evaluate Qwen2.5-VL [6], Qwen3-VL [6], InternVL2 [14], InternVL3.5 [14], LLaVA-OneVision [33], LLaVA-Video [76], and Ovis2 [42], covering their variants with difference scales.

The handling of the video frames modality varies by model. For all open-source models and the GPT series, we uniformly sample 32 frames per video as input. The Gemini-2.5-Pro model is the primary exception, as it supports native video ingestion, allowing us to provide the full MP4 file directly. See Sec. F.2 for more detailed discussion for this. Additionally, for models accessed via the OpenAI API (e.g. GPT series), we enable the low-quality image mode, which forces each frame to be processed at a fixed cost of 85 tokens.

The input for all models follows a standard structure: “[Pre-prompt][Question][Post-prompt][Video Frames]”. The specific prompt templates for NA(Numerical Answers)

Prompts

Pre-prompt:

“These are frames of a video. In the video, objects are identified by numeric tags shown nearby. With that in mind, please answer the following question based on the video.”

Question:

NA: question_text.

MCA: question_text + options.

Post-prompt:

NA: “Your answer must be only the final numeric value, without units or any other text.”

MCA: “Your answer must be only the single letter (e.g., A, B, C, or D) of the correct option.”

Figure 10. Prompts employed when constructing inputs for evaluations.

and MCA(Multiple Choice Answers) are detailed in Fig. 10.

E.2. Metrics and Baselines

Although the prompt explicitly instructs the models to output only the final answer, we implement a regex-based fallback mechanism to handle non-compliant outputs. This parser extracts the last occurring numerical value or a valid multiple-choice option from the full generated text.

We employ two distinct metrics based on the answer format: standard *Accuracy* (ACC) for MCA questions, and *Mean Relative Accuracy* (MRA) for NA questions. MRA measures the proportion of predefined error thresholds that the Mean Relative Error (MRE) can pass:

$$MRA = \frac{1}{10} \sum_{e \in \mathcal{C}} \left(\frac{|\hat{y} - y|}{y} < e \right), \quad (2)$$

where \hat{y} and y denote the prediction and ground truth, respectively, and $\mathcal{C} = \{0.05, 0.10, \dots, 0.50\}$ is the set of 10 error thresholds. This metric results in a step-wise score.

A special consideration is required for dynamic tasks where a near-zero ground truth makes the MRE denominator numerically unstable. We address this by defining a small threshold, \mathcal{ST} . For any ground truth $y < \mathcal{ST}$, a prediction $\hat{y} < \mathcal{ST}$ is awarded a full score of 1.0. If the prediction is incorrect ($\hat{y} \geq \mathcal{ST}$), the MRE is calculated with the denominator floored to \mathcal{ST} to avoid division by zero. This threshold is set to a small value in practice, ensuring it only affects genuinely stationary or near-stationary cases.

For the four-choice MCA tasks, the chance-level baseline is 0.25. In contrast, we define the baseline for all NA tasks as *zero*. This is because, for an uninformed

guesser agnostic to the data distribution, the answer space is effectively unbounded—potentially ranging from centimeters to hundreds of meters—making any specific numerical guess fundamentally arbitrary. We argue that alternative baselines, such as the “Frequency Chance Level” proposed by [65], are invalid as they represent a data leak from the ground truth distribution.

E.3. Human Evaluation Setup

The human evaluation subset is a balanced collection of 270 questions, created by uniformly sampling 30 questions from each of our nine tasks. To ensure a consistent and high-quality evaluation, human annotators were given the instructions in Fig. 11.

Our human evaluation protocol follows the methodology of [65], allowing annotators unrestricted control over video playback (e.g., play, pause, re-watch) to gather comprehensive information. Additionally, we employ a calibration phase (or “warm-up” phase) specifically for open-world scenes, as we recognize the difficulty for human annotators to estimate real-world metric values based solely on visual inputs without training. Five human evaluators complete the entire subset independently and their scores are averaged to get the final human performance.

E.4. Details of Synthetic Scenes.

We generated our synthetic indoor data using the Blender Engine. First, we manually modeled 20 distinct indoor scenes spanning common layouts like washrooms, bedrooms, and living rooms. These scenes featured objects with conventional, real-world scales. We then leveraged the engine’s internal metadata (e.g., object dimensions and locations) to automatically generate 120 template-based questions for our **Normal Set**, covering object size and distance tasks. Next, we created a parallel **Abnormal Set** to serve as our testbed. For each of the 20 scenes, the object scales were deliberately manipulated to be counter-intuitive (e.g., a tiny bathtub, an oversized plant). Crucially, the overall scene layout and camera positions were kept identical to the Normal Set, isolating the variable of object scale. The same automated QA generation pipeline was then applied to this altered metadata to produce a corresponding set of 120 questions.

In the generated video, the camera is positioned at the room’s center and performs two full 360-degree pans to ensure complete object coverage: the first pan is executed with a downward tilt, and the second with an upward tilt. Human evaluators for this test followed the same instructions as in the main evaluation.

See Fig. 12 for a sample of our synthetic test set and Tab. 6 for detailed results.

Model	Task	Normal	Abnormal	Drop (Δ)
Gemini-2.5-pro	Distance	37.3	33.2	4.1
	Size	54.7	29.7	25.0
	Overall	46.0	31.4	14.6
Qwen2.5-VL-32B-Instruct	Distance	43.0	33.0	10.0
	Size	54.5	28.3	26.2
	Overall	48.8	30.7	18.1
Human Performance	Distance	51.7	51.4	0.3
	Size	62.5	60.5	2.0
	Overall	57.1	56.0	1.1

Table 6. Performance Degradation from Normal to Abnormal Conditions.

E.5. Details of Geometric Information Test

To design this experiment, we first sampled *absolute distance* questions from OpenBench, filtering for cases where the two queried objects are not co-visible in any single frame. This selection criterion necessitates that the model reason using camera ego-motion, rather than simply calculating the distance between two objects in a static image. For this specific subset of questions, we then extracted the raw metadata (p_1, p_2, t_1, t_2, R, T) from our pipeline’s intermediate outputs and formatted the tasks as shown in Tab. 7.

F. More Results

F.1. Full Evaluation Results

In addition to the key results shown in the main paper, we evaluated other models such as the full InternVL2 series [14] and Qwen2.5VL series [6]. We provide the comprehensive results for all generalist models tested in our study in Tab. 8.

During this extensive evaluation, we found that two models, Claude-4-Sonnet and Grok5 (with 8-frame input), exhibited collapsed performance. This was due to a consistent failure to adhere to the task’s prompt instructions, rather than a specific failure in spatial reasoning.

F.2. Effects of Input Frames

For all evaluated models, with the exception of the Gemini family, we uniformly sample 32 frames per video as image inputs. These frames are presented chronologically, and the prompt is augmented with temporal information (e.g., video duration and number of sampled frames) to enable time-related reasoning. The Gemini family is the primary exception, as it supports native video ingestion; we provide the full MP4 file directly, as we consider this an integral part of its capability. A second exception is Grok-5, which was limited to 8 frames due to the constraints of the API we used.

We then conducted an ablation study to quantify the impact of frame count on performance, using Qwen3VL-32B (the top-performing open-source model) as our testbed. The

Human Annotator Instructions

- Annotators are permitted unrestricted control over video playback. This includes the ability to play, pause, scrub the progress bar, and re-watch the video multiple times for each question to ensure their answer is as accurate as possible.
- The provided object captions (class names) may occasionally be imprecise. In cases of a conflict or discrepancy between the textual caption and the numerical ID tag shown in the video, the numerical ID should be considered the definitive ground truth. The object designated by the visual ID tag is the correct target for the question.
- For Numerical Answer (NA) tasks, provide the numerical value only, without any units (e.g., 12). For Multiple-Choice Answer (MCA) tasks, provide only the corresponding capital letter of the correct option (e.g., A).
- Before beginning the formal evaluation, annotators are provided with a calibration set. This set consists of 2 sample videos, their 20 corresponding question-answer pairs, and the associated ground truth (GT) answers. Annotators are instructed to review this material to familiarize themselves with the camera properties, the various question types, and to gain a reasonable sense of the metric scales used in the benchmark. This step ensures all annotators are properly calibrated before proceeding to the main evaluation tasks.

Figure 11. Human annotator instructions for evaluation.

Component	Content
Question	What's the distance between the center of the $\{A_class\}$ (id: $\{A_id\}$) and the $\{B_class\}$ (id: $\{B_id\}$) in meters?
Formula post-prompt	In camera coordinates, x points right, y points down, and z points forward. To solve this, apply the following formula: $Distance = \ (R \cdot p_2 + T) - p_1\ $. In this formula, p_1 is the 3D position in the camera coordinate of first queried object observed at the earlier time t_1 , and p_2 is the 3D position of second queried object observed in the camera coordinate at the later time t_2 . The matrix R and vector T represent the rotation and translation the camera pose has changed at time t_2 relative to time t_1 . If any piece of information required to use the formula is not present in the text, you must infer it from the video and then use it in the formula.
Obj1 Info	At $\{t1\}s(t_1)$ of the video, $\{B_class\}$ (id: $\{B_id\}$) is located at $p_1 = [\{p1_x\}, \{p1_y\}, \{p1_z\}]$ meters relative to the camera.
Obj2 Info	At $\{t2\}s(t_2)$ of the video, $\{A_class\}$ (id: $\{A_id\}$) is located at $p_2 = [\{p2_x\}, \{p2_y\}, \{p2_z\}]$ meters relative to the camera.
Ego-motion Info	Between $\{t1\}s(t_1)$ and $\{t2\}s(t_2)$, the camera's relative translation is $T = [\{T_x\}, \{T_y\}, \{T_z\}]$ and the rotation matrix is $R = [[\{R11\}, \{R12\}, \{R13\}], [\{R21\}, \{R22\}, \{R23\}], [\{R31\}, \{R32\}, \{R33\}]]$.
Setting	Question Template
Vanilla	$\{Question\} \{Formula post-prompt\}$
+ One Localization(p_1)	$\{Obj1\} \{Question\} \{Formula post-prompt\}$
+ Both Localization(p_1, p_2)	$\{Obj1\} \{Obj2\} \{Question\} \{Formula post-prompt\}$
+ Ego-Motion(R, T)	$\{Ego-motion\} \{Question\} \{Formula post-prompt\}$
+ All(p_1, p_2, R, T)	$\{Obj1\} \{Obj2\} \{Ego-motion\} \{Question\} \{Formula post-prompt\}$
+ All(w/o Formula)	$\{Obj1\} \{Obj2\} \{Ego-motion\} \{Question\}$

Table 7. Templates for the Geometric Information Test.



(a) Normal scene.



(b) Abnormal scene. From the same perspective.

Figure 12. Samples from our synthetic test set.

results, shown in Tab. 9, indicate that while increasing the number of sampled frames yields a slight performance benefit, the overall gain is marginal.

F.3. Results of Spatial Models

As a comparison, we also evaluated three specialized spatial models: SpatialRGPT-VILA1.5-8B [15], Space-Thinker-Qwen, and SpaceOm [13] (the latter two finetuned on Qwen2.5-VL-3B). The results are presented in Tab. 10. We warn, however, that these scores are not a direct, like-for-like comparison due to fundamental misalignments in task design. SpatialRGPT is a region-prompted model, and to adapt it to our whole-video tasks, we provided a full-image mask as input to give access for the whole depth map to the model. Similarly, SpaceThinker and SpaceOm were not specifically trained for video-based reasoning, which may explain their performance relative to their base models. Therefore, these results are reported primarily as an initial reference.

F.4. Detailed Results of the Comparison for Model Generations

See Tab. 11 and Tab. 12 for the detailed results comparing the QwenVL and InternVL families across different sizes and generations on both OpenBench and VSI-Bench. While a direct, like-for-like comparison at each model size is con-

strained by model availability, two primary findings emerge from this data: (i) on OpenBench, the relationship between performance and model size is non-monotonic, often saturating or degrading; and (ii) the performance gain from newer generations on OpenBench is marginal, which stands in stark contrast to the significant and stable gains reported on VSI-Bench (e.g. >+23.0 for both families and all sizes).

Our main paper’s analysis focuses on the comparison between OpenBench and VSI-Bench [65], as their shared video modality and tasks allow for a direct comparison. To validate that our findings regarding illusory progress on indoor benchmarks are not an artifact of VSI-Bench alone, we conducted an additional test on the multi-view indoor spatial benchmark, All-Angle-Bench [69]. The results in Tab. 13 confirm that the trend of performance gains from larger model scales and newer model generations persists on this benchmark as well. However, the magnitude of the gain from newer model generations is less significant than that observed on VSI-Bench. We hypothesize that this reduced gain may be due to the models’ lack of specific training for the multi-view data format required by All-Angle-Bench.

	InternVL2	InternVL3.5	QwenVL2.5	QwenVL3
2B	21.7	21.7	—	17.1
3B/4B	21.7	23.7	24.2	21.1
7B/8B	24.5	28.5	27.1	31.2
14B/26B	26.0	28.5	—	—
32B ¹	22.9	26.9	30.0	32.2
72B/76B	25.5	—	26.5	—

¹ This line also includes 38B/40B for InternVL series.

Table 11. Comparisons of models on OpenBench across size and generations.

	InternVL2	InternVL3.5	QwenVL2.5	QwenVL3
2B	26.7	52.8	—	53.9
3B/4B	33.5	56.6	27.9	58.4
7B/8B	37.6	56.1	36.8	59.4
32B ¹	37.3	61.4	37.7	61.5

¹ This line also includes 38B/40B for InternVL series.

Table 12. Comparisons of models on VSI-Bench [65] across size and generations.

	InternVL2	InternVL3.5	QwenVL2.5	QwenVL3
2B	40.9	45.9	—	44.6
3B/4B	43.2	49.0	42.7	49.2
7B/8B	47.7	52.1	48.5	50.9
14B/26B	50.3	51.0	—	—
32B ¹	50.8	53.7	54.6	55.7
72B/76B	50.9	—	55.1	—

¹ This line also includes 38B/40B for InternVL series.

Table 13. Comparisons of models on ALL-Angles-Bench [69] across size and generations.

G. Privacy

To address privacy concerns, our data acquisition was conducted exclusively in publicly accessible locations. Subsequently, all collected data underwent a rigorous human curation process to identify and remove any potentially sensitive or private information.

Methods	Rank	Avg.	Relational(\mathcal{MCA})		Static Metric(\mathcal{NA})		Dynamic Metric(\mathcal{NA})			
			Rel. Dis.	Rel. Dir.	Qual. S-Motion	Obj. Loc.	Abs. Dis.	Depth Count	Abs. Disp.	Abs. Speed
<i>Against Human on tiny</i>										
Human-level	-	60.3	85.7	83.3	73.7	43.9	39.2	67.5	42.9	65.8
Gemini-2.5-Pro	-	36.8	53.1	23.1	46.7	39.7	33.8	40.3	22.2	27.8
GPT-5	-	27.9	37.5	30.8	40.0	35.3	25.3	12.8	9.2	31.4
Qwen2.5VL-32B-Instruct	-	32.1	68.8	23.1	33.3	14.4	29.7	31.3	17.5	32.8
<i>Closed-source Models</i>										
Gemini-2.5-Pro	-	37.2	50.0	28.1	52.5	37.4	28.1	37.9	26.8	31.1
Gemini-2.5-Flash	-	19.5	17.9	2.8	50.6	22.7	16.1	26.8	8.1	6.8
GPT-5	-	29.7	34.4	33.1	49.5	32.5	23.7	20.9	10.5	33.8
GPT-4o	-	25.9	30.8	29.1	42.2	22.9	27.0	21.6	17.5	15.5
Claude-3.7-Sonnet	-	26.5	38.9	32.8	47.6	31.3	22.4	31.5	5.2	30.1
Doubaoo-Seed-1.6V	-	27.3	35.9	24.1	44.0	16.6	18.9	38.7	25.7	31.8
Claude-4-Sonnet	-	13.2	7.2	0.7	2.8	20.0	21.6	26.4	9.0	17.9
Grok5(8f)	-	13.6	23.5	19.6	2.1	10.1	10.5	24.2	12.8	13.9
<i>Open-source Models</i>										
InternVL2-1B	-	19.6	33.2	32.1	40.8	7.6	15.4	21.8	7.1	14.3
InternVL2-2B	-	17.1	30.4	18.6	40.6	7.0	7.8	32.9	4.7	13.2
InternVL2-4B	-	21.7	27.2	28.1	40.6	14.6	21.0	36.9	12.2	17.2
InternVL2-8B	-	24.5	35.1	31.7	40.8	21.8	17.8	39.7	15.0	17.8
InternVL2-26B	-	26.0	34.5	34.0	40.7	28.9	20.6	38.3	12.3	23.6
InternVL2-40B	-	22.9	36.7	21.0	41.9	21.1	19.2	33.0	10.0	22.0
InternVL2-76B	-	25.5	32.3	30.6	41.3	15.8	13.5	39.9	15.3	25.0
InternVL3.5-1B	-	19.0	33.4	33.0	36.5	2.4	1.0	28.1	7.0	14.8
InternVL3.5-2B	-	21.7	34.8	32.1	40.1	3.8	2.7	40.8	11.5	16.6
InternVL3.5-4B	-	23.7	37.6	32.8	44.8	4.6	6.7	40.7	15.6	23.4
InternVL3.5-8B	-	28.5	37.6	33.6	47.3	12.2	13.2	42.3	20.3	30.2
InternVL3.5-14B	-	28.5	40.3	33.9	47.1	15.5	15.6	42.8	21.8	32.1
InternVL3.5-38B	-	26.9	40.2	34.0	45.3	11.6	7.7	42.7	20.3	31.4
Qwen2.5VL-3B-Instruct	-	24.2	30.3	32.7	43.0	17.2	26.1	18.4	13.3	19.1
Qwen2.5VL-7B-Instruct	-	27.1	33.1	17.3	41.5	22.0	25.1	27.6	18.3	26.5
Qwen2.5VL-32B-Instruct	-	30.0	41.7	32.7	44.4	23.9	24.0	27.7	16.7	32.8
Qwen2.5VL-72B-Instruct	-	26.5	38.5	20.1	46.5	27.7	26.0	29.4	9.4	29.7
Qwen3VL-2B-Instruct	-	18.4	33.7	32.4	37.5	2.2	4.2	22.4	6.6	19.0
Qwen3VL-4B-Instruct	-	21.1	34.8	23.7	46.4	3.9	6.9	24.1	13.6	20.4
Qwen3VL-8B-Instruct	-	31.2	38.3	31.2	49.3	21.0	15.1	33.3	21.3	34.3
Qwen3VL-32B-Instruct	-	32.2	41.9	28.8	47.1	25.3	11.5	30.2	18.6	36.8
Qwen3VL-30B-A3B-Instruct	-	29.3	37.5	29.9	44.0	12.4	8.7	33.1	20.4	31.7
LLaVA-OneVision-0.5B	-	19.6	27.9	23.8	40.8	13.5	13.1	19.9	10.3	13.6
LLaVA-OneVision-7B	-	25.7	35.1	32.7	40.8	16.1	25.5	25.6	16.8	28.3
LLaVA-OneVision-72B	-	26.9	38.6	32.2	41.7	19.6	18.3	35.3	19.2	23.0
LLaVA-Video-Qwen2-7B	-	22.9	37.1	31.2	40.9	17.6	22.1	18.2	17.5	19.0
LLaVA-Video-Qwen2-72B	-	28.3	39.8	31.1	42.2	23.5	18.0	34.2	20.7	29.9
Ovis2-4B	-	25.9	34.6	30.3	40.1	16.1	18.6	36.8	17.7	22.6
Ovis2-16B	-	28.1	37.0	35.8	42.0	20.0	6.2	41.7	21.7	23.3
Ovis2-34B	-	26.8	37.3	35.5	40.8	19.1	13.1	37.5	18.7	27.4

Table 8. Full Evaluation results for all MLLMs we tested.

Num. of Frames	Avg.	Relational		Static Metric		Dynamic Metric			
		Rel. Dis.	Rel. Dir.	Qual. S-Motion	Obj. Loc.	Abs. Dis.	Depth Count	Abs. Disp.	Quan. S-Motion
8	30.2	40.6	29.7	47.4	21.9	12.6	29.2	18.5	32.0
16	31.8	42.2	29.7	47.3	23.3	11.5	31.0	20.5	35.6
32	32.2	41.9	28.8	47.1	25.3	11.5	30.2	18.6	36.8
64	32.5	42.8	30.2	47.0	26.6	10.4	31.6	17.5	36.5

Table 9. Ablation study on the number of sampled input frames for Qwen3-VL-32B.

Model	Avg.	Rel. Dis.	Rel. Dir.	Qual. S-Motion	Obj. Loc.	Abs. Dis.	Depth Count	Abs. Disp.	Abs. Speed	Quan. S-Motion
		Relational	Static Metric			Dynamic Metric				
VILA-1.5-8B	20.4	30.5	30.0	40.8	17.7	25.2	17.1	15.9	8.8	1.3
SpatialRGPT-VILA-1.5-8B	24.0(+3.6)	31.9	33.0	40.8	23.1	16.1	26.0	19.5	13.9	15.5
Qwen2.5VL-3B-Instruct	24.2	30.3	32.7	43.0	17.2	26.1	18.4	13.3	19.1	21.1
SpaceThinker-Qwen-3B	21.7(-2.5)	29.3	31.9	40.8	0.2	0.3	38.4	6.2	28.0	23.6
SpaceOm-3B	23.2(-1.0)	29.8	26.3	44.0	13.0	23.4	26.5	16.1	22.6	8.5

Table 10. Results for Specialized Spatial Models and Their Corresponding Base Model.



Relative Distance:

Choose from sign board(id:1), electrical housing(id:4), green bench(id:5) and electrical housing(id:6): which one is the closest to street lamp(id:2)?

Answer: electrical housing(id:6)

Relative Direction:

If I am standing by electrical housing(id:6) and facing electrical housing(id:4) is sign board(id:1) to my front-left, front-right, back-left, or back-right?

Answer: back-left

Qualitative Ego-Motion:

Which one best describes the camera's overall movement throughout the entire video? Choose from 'straight', 'left turn', 'right turn' or 'U-turn'.

Answer: left turn

Object Localization:

At 10 seconds into the video, what is the Euclidean distance of the electrical housing(id:4) from the camera in meters?

Answer: 22

Absolute Distance:

What's the distance between street lamp(id:2) and electrical housing(id:6) in meters?

Answer: 4

Depth-Aware-Counting:

At 17 seconds into the video, how many trees are visible within 20 meters from the camera?

Answer: 2

Absolute Displacement:

What is the displacement distance of girl in pink (id:3) between 3s and 7s of the video in meters?

Answer: 8.9

Absolute Speed:

What is the average speed of girl in pink (id:3) between 4s and 6s of the video in m/s?

Answer: 2.1

Quantitative Ego-Motion:

How long has the camera travelled throughout the entire duration of the video in meters?

Answer: 36

Figure 13. OpenBench examples.(Part 1)



Relative Distance:

Choose from vacuum(id:1), fire extinguisher cabinet(id:3), square pillar(id:4) and fire extinguisher cabinet(id:6): which one is the closest to fridge(id:2)?
Answer: fire extinguisher cabinet(id:3)

Relative Direction:

If I am standing by square pillar(id:4) and facing fire extinguisher cabinet(id:6), is vacuum (id:1) to my front-left, front-right, back-left, or back-right?
Answer: back-right

Qualitative Ego-Motion:

Which one best describes the camera's overall movement throughout the entire video? Choose from 'straight', 'left turn', 'right turn' or 'U-turn'.
Answer: U-turn

Object Localization:

At 5 seconds into the video, what is the Euclidean distance of the fridge(id:2) from the camera in meters?
Answer: 4

Absolute Distance:

What's the distance between sign board(id:7) and vacuum(id:1) in meters?
Answer: 38

Depth-Aware-Counting:

At 22 seconds into the video, how many tables are visible within 15 meters from the camera?
Answer: 1

Absolute Displacement:

What is the displacement distance of person in black(id:5) between 7s and 12s of the video in meters?
Answer: 9.8

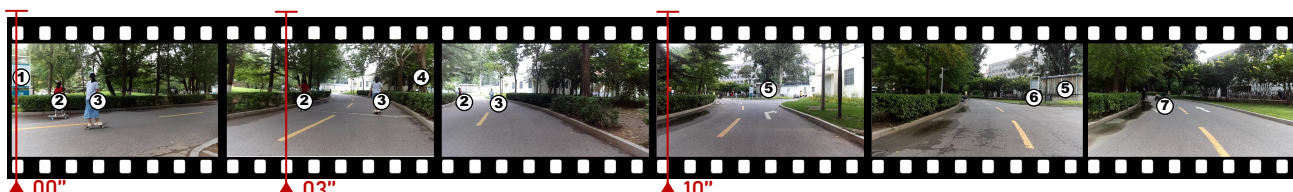
Absolute Speed:

What is the average speed of person in black(id:5) between 7s and 9s of the video in m/s?
Answer: 1.9

Quantitative Ego-Motion:

How long has the camera travelled throughout the entire duration of the video in meters?
Answer: 47

Figure 14. OpenBench examples.(Part 2)



Relative Distance:

Choose from tree(id:4), sign board(id:1), electrical housing(id:5) and vehicle(id:7): which one is the closest to sign board(id:6)?
Answer: electrical housing(id:5)

Relative Direction:

If I am standing by sign board(id:1) and facing tree(id:4), is electrical housing(id:5) to my front-left, front-right, back-left, or back-right?
Answer: front-right

Qualitative Ego-Motion:

Which one best describes the camera's overall movement throughout the entire video? Choose from 'straight', 'left turn', 'right turn' or 'U-turn'.
Answer: left turn

Object Localization:

At 0 seconds into the video, what is the Euclidean distance of the fridge(id:2) from the camera in meters?
Answer: 7

Absolute Distance:

What's the distance between sign board(id:6) and electrical housing(id:5) in meters?
Answer: 4

Depth-Aware-Counting:

At 10 seconds into the video, how many trees are visible within 10 meters from the camera?
Answer: 2

Absolute Displacement:

What is the displacement distance of girl in red(id:5) between 0s and 5s of the video in meters?
Answer: 16

Absolute Speed:

What is the average speed of girl in white(id:3) between 3s and 5s of the video in m/s?
Answer: 3.5

Quantitative Ego-Motion:

How long has the camera travelled throughout the entire duration of the video in meters?
Answer: 31

Figure 15. OpenBench examples.(Part 3)



Figure 16. **Samples showing the workflow of the Joint-Annotation Module.** In the actual implementation, multiple keyframes are processed for each scene.